SYNTHESIS AND CHARACTERIZATION OF SILVER SULPHIDE-REDUCED GRAPHENE OXIDE NANOCOMPOSITE FOR APPLICATION IN THE PHOTOACTIVE AND HOLE TRANSPORT LAYERS OF ORGANIC SOLAR CELLS

OYUGI NGURE ROBERT

A Thesis Submitted to the Graduate School in Partial Fulfillment of the Requirements for the Award of the Master of Science Degree in Physics of Egerton University

EGERTON UNIVERSITY
JULY 2025

DECLARATION AND RECOMMENDATION

Declaration

This thesis is my original work and has not been presented at this university or any other for the award of a degree.

Signature  Date. 10/07/2025

Oyugi Ngure Robert

SM13/13636/19

Recommendation

This thesis has been submitted with our approval as University supervisors.

Signature  Date…14/07/2025.....

Dr. Tabitha A. Amollo, PhD

Physics Department

Egerton University

Signature 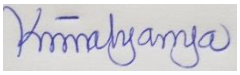 Date …11/07/2025.....

Dr. Kallen M. Nalyanya, PhD

Physics Department

Egerton University

DEDICATION

I dedicate this thesis to myself for not giving up during my study, despite the challenges I experienced. I also dedicate the thesis to my wife, Milca Mildred Awino, for the moral support, to my young daughters Tirzah Mich and Pristine Dorcas, for making me see the seriousness in continuing with my work.

ACKNOWLEDGEMENTS

I acknowledge the help of God with a sound mind and good health throughout this work. I am greatly indebted to Egerton University, especially the Physics Department, for the opportunity to do my studies there. I acknowledge the World Academy of Science (TWAS) and the Future Africa Research Leadership Fellowship (FAR-LeaF) for research funding. I also recognise my supervisors, Dr. Tabitha A. Amollo and Dr. Kallen Mulilo Nalyanya, from the Physics Department at Egerton University, for their continual guidance throughout the development of this thesis. I also acknowledge the University of KwaZulu-Natal, Nanotechnology platform, South Africa, where X-ray Diffraction analysis, thermal gravimetric analysis, and Fourier transform infrared spectroscopy were done. I acknowledge BESSY II at Helmholtz-Zentrum Berlin (HZB), Germany, for assisting with Scanning Electron Microscopy measurements and summer school sponsorship. I acknowledge Mr. Jeremano Ndiritu Maina, who assisted me with laboratory work. I also thank Mr. Vincent Bungei, Masters student, Physics Department, Egerton University, for his support throughout the synthesis and fabrication process.

ABSTRACT

The demand for clean energy, occasioned by technological innovations, necessitates sustainable and cost-effective sources such as organic solar cells (OSCs), specifically bulk heterojunction polymer solar cells (BHPSCs). Inadequate light absorption and charge transport are the common challenges with these sources, which reduce their power conversion efficiency. Incorporating silver sulphide (Ag_2S) and reduced graphene oxide (rGO) can improve light absorption and charge carrier mobility, respectively. The study reports successful synthesis, characterisation, and application of Ag_2S-rGO nanocomposite (synthesised by chemical reduction method) to enhance the OSCs' performance. Scanning electron microscopy (SEM) demonstrated the intercalation of rGO sheets within the Ag_2S nanoparticles during the chemical reduction process, and that Ag_2S had a nanowire shape. Further, SEM energy dispersive X-ray (SEM EDX) showed purity of $Ag_2S - rGO$ by indicating C, Ag, O, and S as the only elements in the nanocomposite. X-ray diffraction (XRD) analysis showed sharp and intense diffraction peaks, confirming the high crystallinity of the Ag_2S nanoparticles. Thermal gravimetric analysis (TGA) showed rGO slowed nanocomposite decomposition between 520°C and 850°C. Ag_2S-rGO nanocomposite exhibited strong absorption of light in the ultraviolet and visible regions, making the nanocomposite suitable for use in OSCs. The Fourier Transform Infrared (FTIR) analysis of the nanocomposite showed strong Ag_2S-rGO interaction with new C-O-C and OH bands, indicating successful integration of rGO into Ag_2S, hence nanocomposite formation. The nanocomposite increased the light trapping of the P3HT: PCBM photoactive layer material within the visible region, improving the efficiency of OSCs in light harvesting. For the hole transport layers, however, the higher rGO content slightly reduced the light transmittance due to strong absorbance and plasmonic effects due to Ag_2S nanoparticles. All the OSCs with modified active and hole transport layers (HTL) exhibited improved photovoltaic performance. The nanocomposite in the absorbing layer improved charge generation, leading to increased *Jsc* (from 6.9 $mAcm^{-2}$ to 17 $mAcm^{-2}$) and a subsequent enhancement in PCE from 1.5% to 3.4% (a 127% increase). The nanocomposite improved charge collection at the interface, leading to an enhanced PCE by 53% (from 1.5% to 2.3%). The application of Ag_2S-rGO nanocomposite considerably improved the performance of the OSCs after application in the HTL and the photoactive layers. Therefore, the study supports the development of sustainable energy solutions.

TABLE OF CONTENTS

LIST OF FIGURES

LIST OF TABLES

LIST OF ABBREVIATIONS AND ACRONYMS

A	Cell area
Ag_2S	Silver sulphide
Ag_2S-rGO	Silver sulphide-reduced graphene oxide
BHJ	Bulk-Hetero-Junction
CVD	Chemical Vapour Deposition
DTG	The Derivative Thermograms
ETL	Electron Transport Layer
FF	Fill Factor
FTM	Floating-Film Transfer Method
GO	Graphene Oxide
HOMO	Highest Occupied Molecular Orbital
HTL	Hole Transport Layer
ITO	Indium Tin Oxide
LSPR	Localised Surface Plasmon Resonance
LUMO	Lowest Unoccupied Molecular Orbital
NPs	Nanoparticles
OSC	Organic Solar Cell
PCBM	(6-6) Phenyl C_{-61} Butyric Acid Methyl Ester
PCE	Power Conversion Efficiency
PHJ	Planar Hetero Junction
PEDOT: PSS	poly(3,4-ethylene-dioxythiophene):poly(styrene sulfonate)
PTB7	poly4,6-(2-ethylhexyl-3-fluorothieno[3,4-b]thiophene-2-carboxylate) alt-2,6(4,8-bis(2-ethylhexyloxy) benzo[1,2-b:4,5-b]dithiophene)
P3HT	Poly-3-hexylthiophene
PSC	Polymer Solar Cells
PVP	Poly Vinyl Pyrrolidone
SEM	Scanning Electron Microscopy
TEM	Transmission Electron Microscopy
TGA	Thermal Gravimetric Analysis
XRD	X-Ray Diffraction

LIST OF SYMBOLS

e	Charge of an electron
E_b	The binding energy of the excitation
I_{sc}	Short-circuit current
I_0	The initial current of the solar cell
J_0	Saturation current density
J_{sc}	Short-circuit current density
η	Power conversion efficiency
η_A	Efficiency of absorption
P_{in}	The incident optical power density
P_{max}	The maximum electrical output power
V_{oc}	Open-circuit voltage

CHAPTER ONE
INTRODUCTION

1.1 Background to the Study

The increase in technological advancement witnessed in the 21st century and global climate change has necessitated clean energy (Dhuriya et al., 2016; Jinfeng et al., 2016). The threat of global warming leading to climate change calls for more sustainable types of energy to replace or minimise the use of fossil fuels and to sustain technological growth and environmental preservation. Fossil fuels are the prime energy sources (Khalil et al., 2016). Besides being detrimental to the environment, they are also on the verge of being exhausted (Dhuriya et al., 2016). Clean energy, also called sustainable, alternative, or non-conventional energy, is energy obtained from natural resources and replenished naturally (Pali & Vadhera, 2016). Clean energy sources include geothermal, hydro, ocean, biomass, wind, and solar (Khalil et al., 2016). The merits of clean sources of energy are that they are inexhaustible and eco-friendly, hence the need to invest in clean energy for the sustainability of the economy (Qazi et al., 2019). Despite the advantages of renewable energy sources, they have their limitations. The main challenge is that clean energy highly depends on the climate (Pali & Vadhera, 2016). The implication is that the amount of clean energy generated in one place may not be the same as in another with different climatic conditions. Secondly, renewable energy sources are still inefficient (Bezrukikh et al., 2016). The improvement of clean energy sources is necessary.

Solar energy, which is abundant in the world, is among the cleanest sources of energy that are useful since it is a reliable green energy source. The cost of this energy source is low because the organic solar cells (OSCs) used in the photovoltaic conversion process are cheaper than their inorganic-based solar cells. Inorganic materials that constitute the dominating solar cells in the market have complex and costly manufacturing procedures (Khalil et al., 2016). The most viable one is OSCs (Amollo et al., 2017; Khalil et al., 2016). The advantages of OSCs are that they are easy and low-cost production methods, enabling low-cost materials to convert solar energy (Dhuriya et al., 2016). However, OSC materials are yet to be fully developed.

There are various reasons for OSCs' poor power conversion efficiency (PCE). The first factor is poor charge mobility. It has been reported that OSCs are plagued with recombination of free charge carriers and poor charge transport (Ray & Alam, 2012). If the mobility is high, the charge carrier will take less time in the device, and hence, loss due to recombination will be

less likely (Mäckel & MacKenzie, 2018). The movement of holes and electrons in OSCs is between 10^{-5} and 10^{-3} $cm^2/V \cdot s$ (Ray & Alam, 2013). Consequently, charge carriers end up piling at the at the interface between the donor and the acceptor, especially when the device's internal field is low during the maximum power condition. An increased offset in quasi-Fermi levels causes the accumulation of free electrons and holes because of poor charge carrier transport (Würfel et al., 2015). High charge recombination will lower the fill factor (FF).

Another challenge with OSCs is poor optical absorption. The prototype OSCs comprise poly-3-hexylthiophene (P3HT): (6-6) phenyl-C_{61}-butyric acid methyl ester (PCBM) in the active layer (Mime et al., 2021). However, P3HT: PCBM has a narrow absorption wavelength (Mime et al., 2021). Most organic semiconductors have wide band gaps starting from 1.9 to 2.2 eV (Oklobia, 2016). This implies limited absorption efficiency (η_A) in OSCs (Arabpour et al., 2018; Kesavan et al., 2016; Oklobia, 2016). As a result, the photocurrent of the OSCs gets limited. One way to enhance light absorption is to use materials with energy band gaps corresponding to a widened range of the spectrum of absorption towards the infrared region (Oklobia, 2016). If the bandgap is high, most of the photons will not cause a photovoltaic effect. There are also other challenges associated with OSCs. The hole transport layer (HTL) of the OSCs is made of poly(3,4-ethylene-dioxythiophene): poly(styrene sulfonate) (PEDOT: PSS), which is soluble in water and acidic in nature (He et al., 2012). This makes it possible for moisture to affect the functionality of the device. The acidity of the HTL may also degrade the active layer underneath.

Nanofilms can overcome the low light absorption and low charge mobility. The internal light scattering has been demonstrated to be improved by thin films to capture more photons inside the solar cells, improving photon harvesting and boosting the PCE of the OSCs (Ohib et al., 2016). Nanoparticles also have the capability of enhancing the low PCE of OSCs. Nanoparticles may be described as a wide variety of materials, including particulate compounds, with a size of less than 100 nm (Ibrahim et al., 2019). The specific and desirable characteristics of nanoparticles result from their small-scale size and the possession of a large surface area. The significance of nanoparticles is that they could facilitate trapping of more light and, consequently, the efficiency of the solar cell in general (Ohib et al., 2016). An example of nanoparticles is silver sulphide nanoparticles (Ag_2S NPs), which use surface plasmon resonance in the visible range for light trapping (Delgado et al., 2018). Additional

characteristics of Ag_2S NPs that cause them to resonate with the requirements of OSCs are a narrow bandgap width (between 0.9 eV and 1.05 eV) (Kumari et al., 2014), high absorption coefficient, monoclinic crystal structure (Hamed et al., 2020), chemical stability, and photoconductivity (Delgado et al., 2018). Ag_2S NPs have also been found to be suitable in photovoltaics through surface plasmon resonances, as they can have enhanced light trapping with the ability to tune resonant wavelengths (Ohib et al., 2016). It was possible that the PCE of OSCs could be further increased by using a silver sulphide-reduced graphene oxide (Ag_2S-rGO) nanocomposite.

Graphene is broadband adsorbing, highly transparent, has high mobility of charge carriers, and high specific surface area, which are critical to high efficiency OSCs (Liu et al., 2017). GO is an oxidised form of graphene, meaning it has the functional groups of oxygen adorning the C basal planes (Perrozzi et al., 2015). GO possesses the structure of oxygen functionalities, including hydroxyl and epoxy at the edges and the basal surfaces that also possess carboxylic groups (Amollo et al., 2018a). Reduced graphene oxide (rGO) is made from GO, and the reduction of GO helps to restore the sp^2 carbon network and also partially restores the graphene's electronic properties, like high charge carrier mobility (Hamed et al., 2020; Hummers & Offeman, 1958). This means that rGO possesses less oxygen content and increased electric conductivity than GO and retains the characteristics of graphene, such as a high surface area (Sharma et al., 2017). The applicability of rGO in OSCs is that the sizes could be tuned to a few nm and 0.1 mm, which enables flexibility of the solar cell devices (Sun et al., 2022). In this paper, Ag2S-rGO was synthesised and applied in OSC HTL and absorber layers. It was envisaged that the synergistic effect of Localised Surface Plasmon Resonance (LSPR) of the NPs and the outstanding properties of rGO would suit the nanocomposite for application in OSCs. To the best of the current literature, no studies were conducted to show how the PCE of OSCs can be improved by applying Ag_2S-rGO nanocomposite to the photoactive layer and HTL.

1.2 Statement of the Problem

The dominant solar cells in the market currently are inorganic solar cells, as they have demonstrated reliable and high-power conversion efficiencies (PCEs). However, their primary drawback lies in the fact that they are costly due to the processes involved in production. For instance, inorganic solar cells use metal oxides in the HTL, which require a vacuum during

production. Inorganic solar cells also require complicated production processes, which further intensifies the cost of production and purchase. It is then necessary to develop solar cells that are affordable. An alternative and cheaper option is to use OSCs. The attractive advantages of OSCs include low fabrication costs, being made from readily available and low-cost materials, being flexible, and being produced in bulk by simple techniques, which are also cost-effective; they are also lightweight and, hence, portable. The challenge with OSCs is that they suffer from low photon absorption and poor mobility of charge carriers, limiting the PCE. Countering these challenges requires development of materials that can enhance the photon harvesting and movement of holes and electrons in OSCs. Despite the existing research, the challenge of movement of charges and trapping of light in OSCs has not been fully addressed. It is against this backdrop that this research aimed at improving the efficiency of OSCs with Ag_2S-rGO nanocomposite in the HTL and photoactive medium.

1.3 Objectives

1.3.1 General Objective

To develop an efficient energy conversion nanomaterial for application in the HTL and photoactive layers of OSCs.

1.3.2 Specific Objectives

i. To synthesise Ag_2S-rGO using the chemical reduction method.
ii. To determine the structural, morphological, as well as optical and electronic properties of Ag_2S-rGO nanocomposite using XRD, SEM, and UV-Vis spectroscopy, respectively.
iii. To fabricate and test the photovoltaic performance of P3HT-PCBM-based OSCs with Ag_2S-rGO in the hole transport and photoactive layers.

1.4 Research Questions

i. Is it possible to synthesise Ag_2S-rGO nanocomposite using the chemical reduction method?
ii. Can XRD, SEM, and UV-Vis spectroscopy be sufficient in determining the structural, morphological, and optoelectronic properties of Ag_2S-rGO nanocomposite?
iii. Does incorporation of Ag_2S-rGO in the active and hole transport layers of P3HT-PCBM-based OSCs impact the device performance?

1.5 Justification of the Study

The development of high-performance OSCs has both scientific and economic benefits. The scientific world is currently focused on finding a lasting solution to global warming. Besides being on the verge of getting depleted, the most commonly used fossil fuels are detrimental to the environment because of the significant role they play in emitting greenhouse gases which lead to climate change. The continued use of fossil fuels has shown that renewable energy sources are inefficient and climate-dependent. This research has contributed to solving this puzzle by developing energy conversion materials designed for efficient OSCs. The main advantage of OSCs is that simple and cost-effective production techniques can be used for fabrication. However, the current challenge with OSCs is that they have low efficiency because of poor light absorption and mobility of charge carriers. This research sought to synthesise, characterise, and utilise Ag_2S-rGO in the active layer and the HTL of the bulk heterojunction polymer solar cells (BHPSCs). The nanocomposite was intended to improve light absorption and enhance the movement of holes and electrons *via* LSPR and the formation of charge percolation pathways, respectively, leading to enhanced PCE. This study enhanced knowledge regarding advancements in energy conversion materials for solar cell applications.

1.6 Definitions of Terms

Different terms have been defined herein to help the reader understand this thesis better.

Annealing: It is heating the cleaned and fabricated samples to remove solvents from the deposited layers.

Bulk Heterojunction Polymer Solar Cell (BHPSC): This is a structure of the polymer solar cell formed by the mixing of the donor and acceptor substances in the photoactive part, forming bulk heterojunctions.

Device: A device is a fabricated solar cell.

Open-circuit voltage: The maximum voltage at which a solar cell can supply power is called the open-circuit voltage, and occurs when no current is taken by the circuit.

Power conversion efficiency: It is the share of solar energy that is effectively harnessed into electricity.

Short-circuit current: It denotes the peak anode current produced by the solar cell when the voltage at the anode is zero.

Short-circuit current density: This is the ratio of short-circuit current to the solar cell area.

CHAPTER TWO
LITERATURE REVIEW

2.1 Introduction

Renewable energy has become one of the main focuses of scientific research worldwide. This follows from the greenhouse effect accompanying the use of fossil fuels (Pantho et al., 2014). There is a consciousness of environmental concerns like rising temperatures, because of CO_2 emissions and fossil fuel depletion (Tzolov & McIntyre, 2017). The advancing research on renewable energy, coupled with the growing world economy, has prompted the need to transition into clean energy investments. The International Energy Agency, having been prompted by the Paris Climate Accord, has forecasted that there will be a six-fold expansion in the production of materials essential to energy from 2020 to 2040 to about 43 million tons yearly (Turner, 2022). Such a projected production is much lower compared to the fossil fuel industry, which generated 15 billion tons of natural gas, oil, and coal during 2020, which, when burned, adds 32 billion tons of CO_2 to the atmosphere (Turner, 2022). As a result, the unprecedented transition to clean energy has become the focus of most economically developing countries (Liao et al., 2021). The focus is to diversify and achieve the sustainability of the energy supply to support economic development.

At the same time, the world is concerned with economic development. It is undeniable that economic growth requires intensive energy use (Kumar et al., 2007). Pollution-free and renewable energy sources are necessary to balance economic growth and environmental conservation. The challenge with the current demand and supply of energy is that it is not sustainable economically, environmentally, and socially (Hosseini & Wahid, 2020). Without conclusive decisions, the increased rates of utilising fossil fuels as a common energy source will heighten the challenges of maintaining secure energy systems and reservoirs alongside the threats of increased greenhouse gas emissions. With the current trends in fossil fuel use as an energy source, greenhouse gas emissions are expected to double by 2050 (Hosseini & Wahid, 2020). Undeniably, this current trend must be changed by delving into sustainable and renewable energy sources. The transition into clean energy is also fuelled by the increasing demand of renewable and clean sources of energy to eliminate the effects of fossil fuels (Arabpour et al., 2018). It is then certain that there is a determination to produce and use clean energy.

However, the transition into clean energy sources is expected to face unprecedented challenges. For instance, Copper, Nickel, and Cobalt, among other materials relevant in energy, usually occur in low-grade ores (Turner, 2022). The implication is that obtaining such materials will require more intensive mining, processing, and waste management issues. Despite these challenges, the transition to cleaner energy is expected to benefit humanity overall. Much of the emissions are expected in the operations, and using cleaner energy sources results in reduced emissions (Carley & Konisky, 2020). The renewable share in the global electricity mix is expected to reach almost 50% by 2050 due to the continued reduction in the prices of solar, wind, and energy storage technologies (Jayachandran et al., 2022). The available technological advances evidence the ability to use renewable energy sources to power the world. There are currently efforts to minimise and eliminate cobalt use, which is toxic, rare to get, and expensive in Li-ion battery systems (Turner, 2022). It means that the storage of harnessed energy from renewable sources is also focused on achieving sustainability.

Developing solar cells is considered an effective way to produce clean energy since it depends on sunlight, which is abundant worldwide and converts it directly to electricity (Arabpour et al., 2018). The sun sends approximately 470 exajoules of energy to the earth in 88 minutes – this is sufficient to supply the total energy requirement of the planet in a year (Jayachandran et al., 2022). In another study, the amount of solar radiation that reaches the surface of the earth is estimated to be 1366 W/m^2, but after the filtering process in the atmosphere on a clear day, an amount of 1000 W/m^2 is estimated to reach the sea level (Rabaia et al., 2021). Such vast energy makes solar energy the most plausible area of interest in achieving clean energy. The solar energy the Earth receives in a few hours is more than enough to power the planet in a year, but the challenge lies in the efficiency of converting that energy to electricity. For this reason, there are advancements in developing the right materials for use in solar cells in a manner that remains friendly to the environment and cost-effective.

The use of solar energy in electricity production is considered a clean source of energy that is cheap and has minimal environmental impact (Mariotti et al., 2020; Najam et al., 2019; Wang et al., 2020). Opposing evidence proves that several environmental challenges are associated with solar power harvesting. One of the problems related to solar energy is that it relies on the weather quality of the weather to convert into electricity. This makes it necessary to have a system that will aid in the storage of the energy, and this ends up increasing the cost of the

solar cell energy (Chanchangi et al., 2021; Farahmand et al., 2021; Rabaia et al., 2021). The solar energy storage equipment processing causes additional energy use, which might burden the environment. Another research revealed that photovoltaic systems are not completely eco-friendly neither do they have absolute zero emissions as the systems pose adverse environmental effects relating to water, land, pollution, and hazard materials used in the manufacturing process of the equipment used (Tawalbeh et al., 2021). Constructing a photovoltaic facility, like any other system for power generation, requires heavy machinery, resulting in disturbances to the natural habitat and the overall environment (Tawalbeh et al., 2021). The manufacturing process also requires using flammable and harmful materials in meagre quantities, and this can pose industrial and environmental risks (Rabaia et al., 2021). The photovoltaic modules also require energy to transport, install, and dispose of, which also come with additional energy consumption other than solar energy, and this might result in adverse environmental impacts when not properly managed (Ratner & Lychev, 2019). The primary concern should, therefore, be whether establishing solar power plants is more beneficial when it comes to emissions.

Most challenges associated with solar power establishment as a clean energy source are common to other investment forms. Development of a solar power plant brings a different set of engineering problems, especially the necessity to consider variable terrain and soil conditions that may affect the overall efficiency and reliability of the plant – an aspect that is usually less important in the development of conventional power plants (Rabaia et al., 2021). Construction of solar power plants can result in habitat loss due to large-area land degradation (Dhar et al., 2020). The consequence of habitat loss would include adverse effects on wildlife and vegetation, which may be serious concerns in developing countries.

The problems associated with environmental challenges from solar energy harvesting can be contained by achieving sustainable energy sources. Considerable landscape modifications are necessary to sustainably ensure no uncontrolled habitat loss (Rabaia et al., 2021). The photovoltaic technology used in solar cells should meet stability, efficiency, and low cost (Arabpour et al., 2018). Through research, there have been emerging thin-film technologies aimed at solving most of the challenges the current commercial photovoltaics face, whereby the intention is to use the earth-abundant nanostructures with simple production and processing methods to ease the impact on the environment and also produce low-cost solar cells

(Zendehdel et al., 2020). Ongoing research has shown that photovoltaic production does not burden the environment.

The most recent advancements in photovoltaic technology are OSCs; they are inexpensive to manufacture and leave little impact on the environment during production. As demonstrated, OSCs can generate large amounts of energy at low cost (Kumar et al., 2007; Liu et al., 2008; Ou et al., 2007; Zhou et al., 2010). The OSCs are also based on organic molecules or polymers; thus, this technology depends on easily accessible materials (Rabaia et al., 2021). OSCs are believed to be cheaper to produce clean energy since thin and flexible devices can be easily made using simple and inexpensive techniques (Liu et al., 2008). These strategies are brush, inkjet, and basic roll-to-roll painting. Maintenance of the device after installation is also not very costly. The problem of OSCs is that they possess low PCEs due to inefficient photon absorption and charge carrier mobility. There is a need to identify materials that shall be integrated into the devices to enhance efficiency in their operations.

2.2 Organic Solar Cells

2.2.1 Common Architectures of OSCs

Two OSC structures are widely used: planar heterojunction (PHJ) and bulk heterojunction (BHJ). PHJ structure is based on patterning the electron acceptor or donor layers in the active layer (Yilmaz et al., 2017). At the planar heterojunction, the acceptor and donor polymer form a bilayer in close contact (Amollo et al., 2020a). In contrast, BHJ architecture has donor and acceptor materials mixed in one matrix, in a highly complicated manner, which enables the formation of nanoscale junctions at the depth of the active layer.

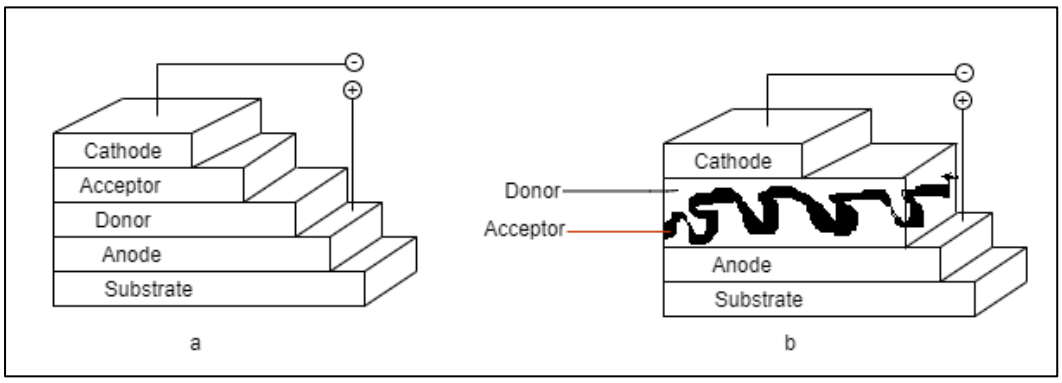

Figure 2.1: (a) Planar and (b) bulk heterojunction OSCs

Figure 2.1 (a) and (b) show these two OSC structures. The PHJ design can be viewed as the most suitable one for flexible solar cells. Nevertheless, they possess lower PCE than the BHJ-organized devices (Kim et al., 2016). The PHJ structures possess a shorter exciton diffusion length of 10 to 40 nm (Amollo et al., 2020a). This is why BHJ is preferable, which is the focus structure of the study.

2.2.2 Importance of Bulk Heterojunction Structure

The BHJ structure is an advanced technology projected to improve OSC's performance in the polymer-based photovoltaic system. The structure was developed to overcome the weakness of the low exciton diffusion length characteristic of polymer solar cells (PSCs) (Amollo et al., 2020a). BHPSCs have an arrangement where the donor and acceptor materials constitute a blend in a bulk heterojunction (Zhou et al., 2010). The BHJ structure may undergo segregation of the acceptor and the donor phase (Amollo et al., 2020a). Such a structure is advantageous for forming excitons in diffusion accessible regions and is favourable for effective carrier separation. This way, the BHJ structure achieves more efficiencies than PHJ. Nonetheless, the earlier solar cells based on bulk heterojunctions had relatively low efficiencies of less than 4% following limitations like poor dissociation of excitons, high recombination losses, and limited light harvesting (Wadsworth et al., 2020). With the development of BHJ, photovoltaics have overcome the challenges, resulting in better efficiencies of above 18% for OSCs (Wadsworth et al., 2020). Another report revealed that since 2000, OSCs have had excellent improvements in power conversion efficiencies from 2% to 18%, which energy level optimizations have majorly occasioned to minimise charge carrier recombination and energy losses alongside maximized light absorption from heterojunction (Ram et al., 2021; Sharma et al., 2022; Zhang et al., 2020). Although the efficiency of OSCs reaches 17% in a laboratory setup, industrial performance and stability remain a significant challenge (Zhang et al., 2020). The significant increase in the performance of OSC is mostly attributed to the advent of BHJ.

2.2.3 Different Layers of Bulk Heterojunction Polymer Solar Cells

BHPSCs' structure comprises a cathode, an electron extraction layer (ETL), an active layer, an HTL, an anode, and a substrate. It is observed in Figure 2.1(b) that the active region is made up of donor and acceptor materials.

i. Cathode

High-performance BHPSCs require an efficient collection of negative charge carriers at the cathode layer. Various materials have been used in making cathodes with the use of aluminium (Al) as one of the most common materials in the process (Deibel et al., 2010; Najam et al., 2019). Other materials are ZnO (Bahrami et al., 2019), LiF/Al, Ca/Al (Deibel et al., 2010), and Barium (Ba) (Gupta et al., 2013). Indium Tin Oxide (ITO), Silver (Ag) (Manzano et al., 2015), and graphene films (Jo et al., 2010) have demonstrated to be useful cathode layer materials.

ii. Electron Transport Layer

This layer ensures sufficient collection of electrons at the cathode (Amollo et al., 2020a). The ETL materials should exhibit good electron collection/hole-blocking properties. Metals or metal salts with low work function, semiconducting metal oxides, and polymers form suitable ETL materials (Agnihotri et al., 2017). However, these materials present various challenges, such as low-work function metals experiencing oxidation at a speedy rate when they are exposed to air (Lattante, 2014).

iii. Active Layer

The BHPSC devices have an interwoven network of donor and acceptor interfaces which form the active layer (Manzano et al., 2015). This layer is usually formed by mixing a polymer with a fullerene, or two different polymers, one of which is the donor, and the other one is an acceptor (Deibel & Dyakonov, 2010). The excitons are made to jump between molecules bridging the donor and acceptor phase before they can either non-radiatively or radiatively recombine (Deibel & Dyakonov, 2010). The dimensions of the phase-separated domains are normally 10-30 nm, which are in line with polymer material exciton diffusion length (Hoppe et al., 2003). Fast excitation also demands the active layer to be present. This can be done by ensuring that the positions of energy levels on the interface enable rapid excitation followed by dissociation of charges rather than recombination with each other (Deibel & Dyakonov, 2010). To have the charge decoupling successfully, it should be noted that the positive charge carriers should remain trapped within the donor matrix but the negative charge carriers should move and accumulate within the acceptor region. The carriers must be moved between the phases prior to their collection without recombination of charges.

Various materials have been used in the active layer. The most commonly used donor polymers are P3HT and poly4,6-(2-ethylhexyl-3-fluorothieno[3,4-b]thiophene-2-carboxylate) alt-2,6(4,8-bis(2-ethylhexyloxy) benzo[1,2-b:4,5-b]dithiophene) (PTB7), while the commonly used acceptor materials are fullerenes PCBM. The main challenge with PCBM is its low absorption of light and hence the lower efficiency of OSCs (Manzano et al., 2015) and difficulty in band gap engineering (Amollo et al., 2020a). In order to release the next-generation performance of devices, the active layer materials must be engineered so that they are not only highly effective at light capture, but also have highly controlled energy levels, namely, high occupied molecular orbital (HOMO) and low unoccupied molecular orbital (LUMO) must be well matched, in addition to the capacity to move holes and electrons rapidly.

iv. Hole Transport Layer

The HTL serves two main functions. The key goal is to enable effective removal of the charge carriers within the donor region of the active layer to the anode, hence reducing the chances of recombination when the charge decoupling has already taken place (Lattante, 2014; Steim et al., 2010). The second function is to reduce the potential barrier at the interface. The organic materials used for the HTL in OSCs include semiconducting PEDOT: PSS (Jeong et al., 2018; N. G. Park et al., 2016) and "Poly[bis(4-phenyl)(2,4,6-trimethylphenyl)amine (PTAA)" (Park et al., 2016). The inorganic materials used for HTL mainly include metal oxides such as molybdenum trioxide (MoO_3) and vanadium pentoxide (V_2O_5) (Jung et al., 2010). However, metal oxide materials have oxygen content, which may degrade the active layer polymer of the solar cell (Jung et al., 2010). Metal oxides also require a vacuum during production, which is not cost-effective.

PEDOT:PSS remains the preferred material as HTL because of its tuneable electrical conductivity, low-temperature compatibility, excellent light transmittance within the wavelength of 300 to 800 nm, high work function, and high optical transparency (He et al., 2012; Vitoratos et al., 2009). PEDOT: PSS can be deposited over the active material by using the method of spin coating at low cost because it is soluble in water (He et al., 2012). The problem lies in the fact that PEDOT:PSS is acidic in nature and this could destroy the active layer beneath (Vitoratos et al., 2009). This could lead to poor performance of the BHPSC. To overcome this dilemma, an additional layer is deposited at the active-HTL interface (Rafique et al., 2017). The non-polymer solvents are the material used to deposit the interfacial layer

that is a conducting polymer. Poly (3,3"-dialkylquaterthiophene) (POT-12) is one of the conducting polymers that may be used as the interfacial layer (Rafique et al., 2017). The main reason to use POT-12 is that it has a good phase matching and the energy band of the material aligns with the active layer (Rafique et al., 2017). This aids in the enhancement of the transportation of charges in the solar cell. The floating-film transfer method (FTM) deposition of the POT-12 layer protects the active layer underneath the POT-12 solvent (Rafique et al., 2017).

Graphene thin films have proved to be effective as HTL material too (Li et al., 2010). The HTL with GO assists in attaining high-performance OSCs (Yun et al., 2011). The GO films are also insulating and this means the performance of the solar cells will be highly determined by the thickness of the GO films (Yun et al., 2011). The advantage of GO in the HTL is that it facilitates more efficient charge transport. Insulating GO film is easily tuneable through thermal/chemical treatment into semi-metallic thermally/chemically reduced graphene oxide (rGO) (Yun et al., 2011). Oxygen removal from the GO induces GO transition to semiconductors from an electrical insulator (Kesavan et al., 2016). Materials based on GO are also advantageous because, in their aqueous suspensions, they can still be quickly deposited, yielding efficiencies that corroborate with the PEDOT: PSS fabricated devices (Kesavan et al., 2016).

v. Anode

This layer collects the positive charge carriers from the active layer donor region. ITO is largely used as an anode because it transmits light effectively, allowing solar radiation to reach the underlying photoactive elements. The material is considered for BHJ because of its easier etching (Najam et al., 2019). Besides being inexpensive and transparent, ITO is lightweight and flexible (Najam et al., 2019). The anode is built on a glass substrate. The substrate should be non-soluble, have low power loss, and not allow recoupling of electrons and holes (Wen et al., 2019).

2.2.4 Working Principle of Bulk Heterojunction Polymer Solar Cells

Another type of photovoltaic is BHPSCs used to convert sunlight energy into electricity. The operation of these solar cells occurs in four key steps that include the incoming light capture, the exciton formation, the dissociation of the bound pair of charges into free charges, and the

transport of the electrons and holes towards their electrodes (Anagnostou et al., 2019). The substrate of the BHPSC absorbs the sunlight in the form of photons when it reaches the photoactive layer (Najam et al., 2019). Photoactive region is a unique material that gives and receives electrons (Manzano et al., 2015). When the donor material in the active layer is absorbing the photons, the electrons can be excited and promoted from the HOMO to the LUMO, and the charge generation process has started (Anagnostou et al., 2019). The negative charge carriers (excitons) are released and the hole (positive charge carriers) is left (Anagnostou et al., 2019). Coulombic forces bind the holes and the electrons together and create an exciton quasiparticle (Anagnostou et al., 2019). Excitons must pass the molecular network of the working layer and arrive at the interface of the donor-acceptor phase and separate the charge to avoid recombination (Lattante, 2014). This requires the donor and the acceptor materials to be fine-mixed in the active layer to devise an optimised BHJ structure (Deibel & Dyakonov, 2010). This is accomplished by ensuring that the phase domains are in 10 nm to 30 nm which is the average length of excitation diffusion in polymers (Deibel & Dyakonov, 2010).

It is also possible to solve recombination of charge carriers in BHPSC with non-fullerene acceptors. Studies have revealed that non-fullerene substances provide the flexibility of tuning the energy band gaps thus displaying minimal power losses and charge carrier recoupling (Cheng et al., 2018). There should also be interface energy levels that can allow the excitons to be dissociated fast (Deibel & Dyakonov, 2010). During the formation of excitations, much power is lost (Brdas et al., 2009). These power losses are unfavourable in cases where low bandgap materials are employed in the collection of photons in the near-infrared wavelengths (Brdedas et al., 2009). Any power loss can be avoided at the photon collection point with high bandgap polymers (Zhou et al., 2010). Excitons are neutral, hence, not influenced by the electric field as they migrate (Br Redas et al., 2009). As a result, the excitons randomly diffuse until they reach the heterojunctions in the active layer. The exciton is further separated into the positive and negative charges along the border of donor and acceptor areas (Anagnostou et al., 2019). After separation, the charge carriers are required to travel in the respective phases until they reach the collecting electrodes without recombination (Deibel & Dyakonov, 2010). The collection and the flow of these charge carriers explain how electric current is generated from the sunlight.

2.3 Performance Parameters of Solar Cells

Photovoltaic performance is determined based on various parameters. These parameters include short-circuit current density (J_{sc}), open-circuit voltage (V_{oc}), fill factor (FF), and power conversion efficiency (ɳ).

i. Short-Circuit Current Density

Short-circuit current density is associated with short-circuit current (I_{sc}). I_{sc} is the maximum current at the anode when the voltage at the anode is zero (Figure 2.2). The values of I_{sc} are dependent on the optoelectrical properties of the material used for the active layer, incident illumination, material used for the electrode, and the materials' structures (Najam et al., 2019). I_{sc} is given by equation (2.1).

$$I=I_{sc}-I_0(e^{\frac{v}{v_T}}-1) \quad (2.1)$$

Here, I denotes the current the solar cell generates, I_{sc} is the short-circuit current, v is the recombination velocity, and I_0 is the initial current in the solar cell.

I_{sc} relates to the current density, $J_{sc,}$ by:

$$I_{sc}= AJ_{sc} \quad (2.2)$$

Here, A is the cell area.

The short-circuit current is defined by the intensity, which is influenced by a variety of operational and material-related factors. First, the I_{sc} has a direct relationship with the irradiance a solar cell receives (Akter et al., 2014; Malti & Sari, 2014). High energy losses due to series resistance also decrease I_{sc}. High series resistance losses reduce the responsivity of the device, thereby limiting I_{sc} (Braun et al., 2012). Therefore, minimising the series resistance losses would improve solar cells' efficiency. The OSCs generally have low I_{sc} because of the high series resistance in these solar cells (Akter et al., 2014). OSCs have a series connection, which makes the sub-cell that generates the least current limit the available solar cell device's current (Reichmuth et al., 2020). This limiting sub-cell is then forced to be operational on the reverse bias. The size of a solar cell is directly proportional to the short-circuit current where the larger the active surface area the more photons are captured and the higher the current density is (Park et al., 2019). A plausible path towards enhancing the performance of solar devices is to raise the J_{sc}, which is given by equation (2.3) (Malti & Sari, 2014).

$$J=J_{sc}- J_0(e^{\frac{v}{v_T}}-1) \quad (2.3)$$

Various ways have been used to enhance J_{sc}. A significant current enhancement has been witnessed with a radiation wavelength of between 400 nm and 750 nm (Kesavan et al., 2016). The efficiency in the collection of the light and the photogeneration of the exciton takes place between these wavelengths. It is also possible to increase the recombination velocity to enhance J_{sc} (Sakib et al., 2017). The problem is that the efficiency and V_{oc} decline with the increase in recombination velocity (Sakib et al., 2017). Thickness, only up to a limit, enhances the efficiency of the solar cells. Once the point is reached, the efficiency begins to decline as the increase in thickness is observed. Incorporating plasmons into the active layer is one of the ways to enhance the efficiency of the solar cells. As an example, the active layer can be enhanced by adding plasmonic and optical spacer materials to enhance the J_{sc} through enhanced absorption, separation, and transport of charge carriers (Amollo et al., 2020a). The change can enhance the efficiency and the working performance of OSCs.

The voltage and current density of the anode of a solar cell is shown in Figure 2.2.

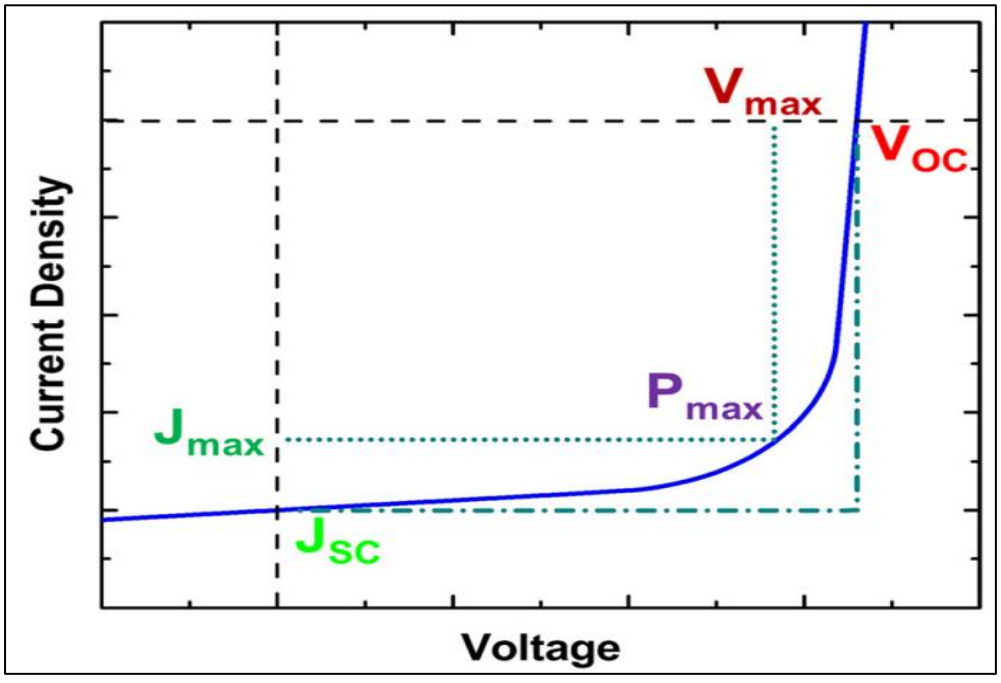

Figure 2.2: Current density -voltage graph for solar cells

Source: Printz and Lipomi (2016)

ii. Open-Circuit Voltage

The V_{oc} is the maximum voltage with no flow of external current (Najam et al., 2019). The V_{oc} may therefore be said to be the maximum voltage that can be read at the anode when the circuit is open and no current is being drawn and is given by equation (2.4).

$$V_{oc}=\frac{1}{e}\left[\left|HOMO_{Donor}\text{-}LUMO_{Acceptor}\right|-\frac{E_b}{2}\right] \quad (2.4)$$

In this context, e refers to the elemental charge carried by an electron, an E_b refers to the binding energy of the exciton. As per Equation (2.4) a linear correlation can be drawn between V_{oc} and the energy level difference between the HOMO of a donor and the LUMO of an acceptor (Chowdhury & Mominuzzaman, 2015).

iii. **Fill Factor**

The Fill Factor of a solar cell is defined as the ratio of the maximum power obtainable divided by the product of the I_{sc} and V_{oc} of the cell. It helps show the cell's absorption efficiency (Ray & Alam, 2013). The FF also shows how efficient charges are collected in solar cells (Najam et al., 2019). The efficiency of charge collection depends on many factors including the recombination rate, charge carrier mobility, and the internal electric field, which drives holes to the anode and electron towards the cathode (Ray & Alam, 2013). In order to achieve high FF, it is important to have adequate compatibility between electron and hole mobilities in order to maintain charge balance in transport. FF is expressed by equation (2.5) (Najam et al., 2019).

$$FF=\frac{P_{max}}{I_{sc}*V_{oc}} \quad (2.5)$$

In equation (2.5), P_{max} is the maximum electrical output power.

OSCs are plagued by poor charge mobility. The charge mobility in OSCs is between 10^{-5} and 10^{-3} $cm^2/V\cdot s$ (Ray & Alam, 2013). In this case, charge carriers will accumulate at the donor-acceptor interface and hence promote geminate recombination which is particularly high under low internal electric field conditions such as those experienced near the maximum power point of the device. This piling up of charge carriers lowers the FF due to the high loss of charge carriers due to recombination.

FF can be improved through various means. Having very high mobility of the charge carriers is one way to enhance FF. The high carrier mobility of orders greater than $10^{-2}cm^2/V{\cdot}s$ makes it possible to achieve more than 80% of FF (Ray & Alam, 2013). The charge mobility can be optimised using highly ordered polymers where the π-π stacking is very close (Guo et al., 2013; Ray & Alam, 2012). FF enhancement can further be achieved by using microstructure in the active layer (Guo et al., 2013). Other methods, such as using graphene for polymer percolation doping, inkjet printing for antisolvent crystallisation, and adding small solvent additive amounts of solvent to the active layer blend, help improve the charge mobility (Ray & Alam, 2012).

iv. **Power Conversion Efficiency**

PCE measures how much power that gets into the device is converted into output. To improve PCE, it is imperative to improve the J_{sc}, V_{oc}, and I_{sc}. Equation (2.6) shows the expression for PCE (Najam et al., 2019).

$$\eta = \frac{J_{sc} * V_{oc} * FF}{P_{in}} \tag{2.6}$$

where P_{in} is the incident optical power density.

The primary causes of poor PCE include low carrier mobility and absorption efficiency. Therefore, the first method to improve the PCE is to use thin films (Tadeson & Sabat, 2019; Zuhir et al., 2017). This method allows for improved mobility of charge carriers and, hence, improved PCE. PCE can further be enhanced by using bulk heterojunctions (BHJs), where the donor and acceptor materials are mixed into a single layer (Karim et al., 2017). Solar cell efficiency can be achieved by carefully optimizing the composition of the active layer (Islam et al., 2019). More improvement is needed in the active layer design for PCE to be optimised.

2.4 Advantages of Organic Solar Cells

OSCs are appreciated in a set of benefits, including the comparably low cost of their production, can be made from readily available and low-cost materials, are flexible, can be produced in bulk using simple and cost-effective techniques (Najam et al., 2019; Shamsudin & Sanip, 2015; Z. Wang et al., 2014; Yamanari et al., 2006). OSCs are also light-weight, hence easily portable (Najam et al., 2019). Low socio-economic status communities can utilise OSCs and have affordable solar power.

2.5 Challenges Associated with Organic Solar Cells

Understanding the associated challenges with using OSCs is necessary in identifying opportunities for improvement. One of the significant challenges is poor PCE. The progress in the development and design of OSCs has been promising, but they still lack commercial viability. This is blamed on the low efficiency of these solar cells. To date, the best PCE of 4.65 percent has been attained through the optimisation of P3HT: $PC_{60}BM$ (Shaban et al., 2021). The optimisation was performed by coating at spin frequencies of 900 to 3000 rpm (Shaban et al., 2021). This is yet a low PCE and it can be improved further.

OSCs are challenged with low optical absorption efficiency. Poor light absorption is the key limitation of the performance of OSCs (Zhang et al., 2010). The issue is that organic semiconductors should be created to be efficient at converting light within the solar spectrum (Pantho et al., 2014). The absorption spectrum of most organic semiconductors is narrow and, therefore, they have low photon absorption (Ou et al., 2007). Solar photon flux is at its peak between the wavelength range of 600 nm to 800 nm (Ou et al., 2007). However, the maximum optical absorption of most polymers is at less than this wavelength. As an example, maximum absorption of Poly[2-methoxy-5-(2-ethylhexyloxy)-1, 4-phenylene vinylene] (MEH-PPV) is at 498 nm (Ou et al., 2007). This is the reason why there is poor light uptake (Pivrikas et al., 2010; Zhou et al., 2010). Light absorption is a limiting factor of PCE in OSCs and therefore devices are needed to be designed to have an absorption that is matched by the solar spectrum to increase PCE. Conversely, the exciton dissociation relies on the active layer blend, the way the phases separate and the LUMO and HOMO energy levels (Hamed et al., 2020). To solve this challenge, BHJ was developed, where BHJ forms an interpenetrating network, enabling the efficient excitation dissociation and, therefore, charge carrier transport (Zhang et al., 2010).

The other reason that leads to poor PCE in OSCs is poor charge mobility. The active layer has a low hole and electron mobility that is identified as a major restraint to the PCE in OSCs (Kalita et al., 2010). Organic semiconductors have low dielectric constants that make the electrostatic attraction between the charge carriers weakly screened to cause a low charge mobility in OSCs (Pivrikas et al., 2010). This minimizes the chances of loss of the charge. With low charge escape probability, charges will not freely escape the electrostatic attraction between them and hence, high recombination rates of the charges (Koster et al., 2005; Lenes et al., 2009; McNeill et al., 2007; Westenhoff et al., 2008). Increased exciton separation refers

to the case whereby the electrons and holes that were bound by their Coulombic interaction become mobile charge carriers and thus increases the yield of mobile charge carriers (Pivrikas et al., 2010). This, in turn, improves the PCE of the OSCs.

2.6 Improving the Power Conversion Efficiency of OSCs

Various methods of PCE improvement have been suggested. Increasing absorption is the first recommended PCE improvement technique. Achieving high efficiency in OSCs requires that the active layer absorbs the highest possible amount of photons (Österbacka et al., 2010; Zhou et al., 2010). Increasing the photon absorption requires a low-bandgap polymer. The reason why low-bandgap compounds are used as the active layer in solar cells lies on the basic principle that only photons whose quantum energies are greater than or equal to the bandgap have the ability to produce photocurrent. Therefore, if the active layer material has a small bandgap, more photons will participate in the generation of electricity, hence high OSC efficiency (Qian & Zhang, 2011; Tzolov & McIntyre, 2017).

The BHJ is also an effective way of improving PCE. Bulk heterojunction acts as a hole and electron selection interlayer, which further enhances the operational efficiency of OSCs (Kalita et al., 2010). BHJ allows for the effective creation of charge percolation paths, thereby minimising disarrangement in the cell that might block charge carriers (Jaehoon et al., 2016). Fullerene derivatives that have long been used in OSCs demonstrate vulnerability to molecule dispersion between the p-type conjugated polymer (Jaehoon et al., 2016). For a BHJ based on the polymer-PCBM blend, the polymer should also be of low HOMO level and bandgap (Qian & Zhang, 2011). Such a combination collaboratively increases the V_{oc} and I_{sc}, improving the solar cell's efficiency.

Carbon nanotubes have been found to be excellent materials to improve the efficiency OSCs. It has been shown that incorporating carbon nanotubes in OSCs improves charge transportation and, hence, the efficiency of device performance (Kalita et al., 2010; Liu et al., 2008). Carbon nanotubes can also be used as electrodes, which help replace brittle and expensive ITO (Liu et al., 2008). The importance of carbon nanotubes is that they can be easily sprayed uniformly to get devices with excellent mechanical flexibility and a large area at a low cost. Nonetheless, the efficiency of carbon nanotubes is still low (Derval et al., 2009). Further improvement is still needed to ensure that the PCE of the OSCs is achieved.

2.7 Application of Nanoparticles in OSCs

It is possible to enhance PCE of OSCs using nanoparticles. This is due to the appropriate qualities of nanoparticles. Another possibility is to augment light-harvesting efficiencies in organic photovoltaics with nanoparticle, and this way retain the compact design of the device (Tran et al., 2015). The technology of nanoparticles provides surface plasmon resonances that increase the light trapping and the possibility of tuning the resonant wavelengths (Ohib et al., 2016). Therefore, nanoparticles enhance light absorption and efficiency of solar cells without reducing the thickness of the film (Ohib et al., 2016). LSPR is used by metal nanoparticles to give enough light trapping in a photoactive medium (Hamed et al., 2020). Silver nanowire electrodes are one of such metal nanoparticles that can make a better OSC (Hamed et al., 2020). Based on these properties, it may be concluded that nanoparticles may contribute to solving the problem of light absorption in OSCs. Due to this reason, n-type semiconductor silver sulphide nanoparticles are taken into consideration in the present studies. Silver sulphide is chosen due to its interesting characteristics about organic solar cells. Among them is monoclinic crystal structure, a high absorption coefficient, low band gap (0.9 eV to 1.05 eV) and chemical stability (Hamed et al., 2020). Silver sulphide possesses high-quality photo-conductivity and electronic characteristics that can be used in photovoltaics (Hamed et al., 2020). To increase the optical and electrical efficiencies of solar cells, nanostructures have also been incorporated with thin-film photovoltaic technology (Choudhury & Chowdhury, 2016).

2.8 Application of Graphene Nanomaterials in OSCs

A lot of research and industrial interest has been on graphene that was isolated in 2004. Graphene is a single layer material of sp^2- hybridised carbon atoms tightly packed in a honeycombed lattice structure. Characteristics of graphene that render it usable in OSCs are high charge carrier mobility, flexibility, high mechanical strength, large surface area, ballistic transport, quantum Hall effect, and ambipolar electric field effect (Amollo et al., 2020a). Graphene is also an alternative to carbon nanotubes because of its distinctive nanostructure and properties (Shiau et al., 2019). Graphene nanomaterials have been used in OSCs' interfacial and active layers (Amollo et al., 2018). Graphene-based photodetectors can also detect photons covering an extensive segment of the solar spectral range (Yogeswaran et al., 2017). This property is highly essential for increasing the absorption of OSCs. Graphene nanomaterials also have higher charge carrier mobility as they allow for a rapid photoresponse after absorption of an incident photon (Yogeswaran et al., 2017). Various plasmonic effects can be

realised by combining graphene with other polarizable nanoparticles (NPs) (Vasilevskiy et al., 2016). Thus, it was envisaged that Ag_2S-rGO nanocomposite would increase the photon harvesting and mobility of charge carriers in OSCs, hence the solar cells' improved PCE.

Graphene oxide (GO) is an oxidised product of graphene with O functional groups which adorn the sp^2 of the basal planes of C (Perrozzi et al., 2015). Besides, GO is hydrophilic, and can be dispersed in water or solvents, but graphene is hydrophobic. It is also possible to tune the sizes of GO widely between a few nm and µm, giving them an advantage in wide applications. GO in its reduced form has been applied in electronic devices, biomedical applications, energy storage, supercapacitors, biosensors, catalysts, water purification, and membranes (Jiříčková et al., 2022). Removing functional groups with oxygen atoms from GO during the reduction process restores the sp^2 graphene-conjugated network, thereby improving electron transport (Amollo et al., 2018b). This makes rGO highly applicable to solar energy conversion. This is why silver sulphide-reduced graphene oxide nanocomposite was expected to have excellent material characteristics necessary for various applications.

Graphene synthesis is also cost-effective, which makes it beneficial for use in OSCs (Amollo et al., 2020a). This has presented an affordable and non-toxic pathway of making GO by optimizing the parameters of the synthesis process including time and temperature (Ranjan et al., 2018). This is done in two ways, the bottom-up and top-down synthesis. The bottom-up route involves the production of graphene with the help of carbonaceous gas feedstock (Lopez et al., 2016). Such a feat is possible with chemical vapour deposition (CVD) and epitaxial growth in Silicon Carbide (Lopez et al., 2016). Conversely, the top-down pathway to graphene production includes the exfoliation and reduction of GO at the same time (Ranjan et al., 2018). This study was to obtain GO, which was further reduced into rGO using the chemical reduction method.

The usual ways of GO reduction are thermal reduction, doping, oxygen-containing functional group removal, and chemical reduction. The thermal reduction occurs without the presence of air, such as in inert conditions or vacuum (Qiu et al., 2014). On the other hand, GO may be transformed into rGO using the aid of doping removers, including ascorbic acid (Tewatia et al., 2021). Chemical reduction is the most popular way of rGO synthesis. Chemical reduction can be conducted on a regular room temperature (Yousefi & Cheraghizade, 2018). Essentially,

the chemical reduction can achieve mass production of rGO (Yousefi & Cheraghizade, 2018), it is cost-effective, has a reasonable production rate (Rahimi & Doostmohammadi, 2020), and allows for regulation of the chemical makeup of the nanomaterial or nanocomposite formed (Virji & Stefaniak, 2014). It is in the backdrop of these advantages that this study used the chemical reduction method for the synthesis of the Ag_2S-rGO. Obtaining homogeneous and stable solutions is also necessary in synthesising nanocomposites based on graphene (Song et al., 2012). Thus, GO was the most appropriate for synthesising the nanocomposite since it has oxygen functional groups below and above the basal planes, providing nucleation sites for doping heteroatoms (Lv et al., 2014). It is imperative to determine the material properties of the formed nanocomposite; hence, this study characterised the Ag2S-rGO nanocomposite before fabricating OSCs.

CHAPTER THREE
MATERIALS AND METHODS

3.1 Synthesis of Graphene Oxide (GO)

A variation of the Hummers method was used for GO synthesis (Hummers & Offeman, 1958). The synthesis started by mixing the precursor materials: 50 ml of concentrated sulphuric acid, 1g of graphite powder, and 1g of sodium nitrate. The temperature was maintained at a constant 0 °C, while the solution was continuously stirred for half an hour and 6 g of potassium permanganate was added. After adding potassium permanganate, the blend was stirred at 35 °C for 3 hours. 200 ml of hydrogen peroxide (3%) was introduced, followed by continued stirring of the solution for 30 minutes (Amollo et al., 2018a). Double-distilled water was used to wash the solution to a neutral pH. The washed solution was dried at 50 °C in a vacuum oven to obtain the GO films.

3.2 Synthesis of Silver Sulphide Nanoparticles and Silver Sulphide-Reduced Graphene Oxide Nanocomposite

The Ag_2S nanoparticles were synthesised following the protocol of Hamed et al. (2020a). The precursor solutions for the synthesis of the nanoparticles included 1.698g (0.1M) of silver nitrate hexahydrate ($Na_2S.6H_2O$), 0.4 g (0.1 M) of sodium sulphide, and 3.0 g of polyvinyl pyrrolidone (PVP), which were separately underwent dissolution in 50 mL of double-distilled water. During a period of three hours, sodium sulphide and PVP solutions were added drop by drop into a solution of silver nitrate with the constant stirring. The obtained precipitate was centrifuged at 4500 revolutions per minute for 5 minutes. The centrifuged precipitate was successfully cleaned with ethanol and double-distilled water until a neutral pH was obtained. The residue was then dried in an oven for 3 hours at 80°C to obtain Ag_2S NPs. For the synthesis of the Ag_2S-rGO nanocomposite, GO at varied concentrations of 10 mg, 100 mg, and 150 mg in 10 ml, 100 ml, and 150 ml of double-distilled water, respectively, was injected into the mixture of silver nitrate, PVP, and sodium sulphide. The mixture was further stirred for 1 hour. The solution obtained was spun at 4500 revolutions per minute for five minutes using a centrifuge and successively washed in ethanol and double-distilled water. The final residue was dried for 8 hours in a vacuum oven at 80°C to obtain the nanocomposite.

3.3 Characterization of the Nanomaterials

A field emission scanning electron microscope (SEM: Phenom Pro by Thermofisher) was used to determine the materials' morphology. The sample was securely attached to the sample holder and appropriately positioned in the SEM machine for the SEM imaging. The SEM machine was then focused at high magnification, above 4000×. The beam was centred, and astigmatism was corrected. The mechanical vibrations of the SEM machine were then minimised as much as possible to help get a quality image. The depth field and working distance were adjusted appropriately for a high-quality image. An Electron Dispersive X-ray Spectroscopy (EDX) detector attached to SEM (Phenom Pro by Thermofisher) was used for elemental analysis. Morphology shows the smoothness of the surface of the nanocomposite.

The structural analysis was done using XRD (MiniFlex 300/600) with Cu Kα radiation (λ = 1.5418740 Å). Powder XRD analysis for the determination of the structure of the Ag_2S-rGO nanocomposite was done with a scanning range of 2θ from 10° to 90° and a scanning speed of 10 °/min. A powder sample was put in the sample holder of the XRD machine. The machine operated where the detector was expected to move around the sample, and the number of X-rays observed after every 2θ. The X-ray intensity was then measured as counts (automatically done by the XRD machine).

The thermal gravimetric analysis (TGA) was used to investigate Ag_2S nanoparticles and Ag_2S-rGO nanocomposite thermal stability. The nanoparticles and the nanocomposite were raised from room temperature to 1000 °C in a nitrogen gas atmosphere. The heating rate was set at 10°C per minute.

Fourier transform infrared (FTIR) was used to analyse the oxygen functional groups in Ag_2S-rGO nanocomposite using Perkin Elmer Spectrum 100 FTIR. A UV-Vis spectrophotometer (UV-1900i by Shimadzu) was used to characterise the optical absorption of the nanomaterials dispersed in ethanol at various wavelengths.

3.4 Solar Cells Fabrication

Ag_2S-rGO nanocomposite was employed in the P3HT: PCBM active layer and HTL of the OSC. For the HTL, the Ag_2S-rGO nanocomposite was dispersed in PEDOT: PSS at concentrations of 20 wt.% and 30 wt.% by overnight stirring at 40 °C to get a homogenous

solution. For the modified photoactive layer, a solution of P3HT: PCBM at a ratio of 1:1 in 20 mg/ml concentrations of chloroform and Ag_2S-rGO at various concentrations of 10, 20, and 30 wt.% was prepared. The solution for the active layer was stirred for 3 hours at a temperature of 40°C.

Devices based on BHJ-OSC with modified HTL were fabricated following the architecture of glass/ITO/PEDOT: PSS: Ag_2S-rGO/P3HT: PCBM/LiF/Al (Figure 3.1a). Similarly, the devices with modified photoactive layers were fabricated in the architecture of glass/ITO/PEDOT: PSS/P3HT:PCBM: Ag_2S-rGO/LiF/Al (Figure 3.1b). Patterned glass substrates coated with 15Ω/sq sheet resistance ITO were cleaned before coating the various layers.

Cleaning the substrates started with ultrasonication in deionised water at 100 °C with a soap solution. The substrates were ultrasonicated in deionised water, acetone, and isopropanol, each for 10 min with uninterrupted magnetic stirring. The substrates were cleaned and dried in an oven at 120 °C for 30 minutes. Spin coating of PEDOT: PSS- Ag_2S-rGO HTL was done for 60 seconds at 4500 rpm. P3HT: PCBM and P3HT: PCBM: Ag_2S-rGO were subsequently spin-coated for 60 seconds at 1200 rpm on the PEDOT: PSS-Ag_2S-rGO and PEDOT: PSS HTLs, respectively. The annealing of the films was done by heating the films at 120 °C for 5 min under flowing nitrogen. LiF (0.4nm) and Al (50nm) were then thermally deposited under vacuum after this (Using an EDWARDS AUTO 306 TURBO thermal evaporator). The vacuum was set at a pressure of 10^{-6} mbar. Reference devices with PEDOT: PSS HTL and P3HT: PCBM active layer were also fabricated for comparison purposes. All the devices were ambient fabricated with a 0.04 cm^2 active area.

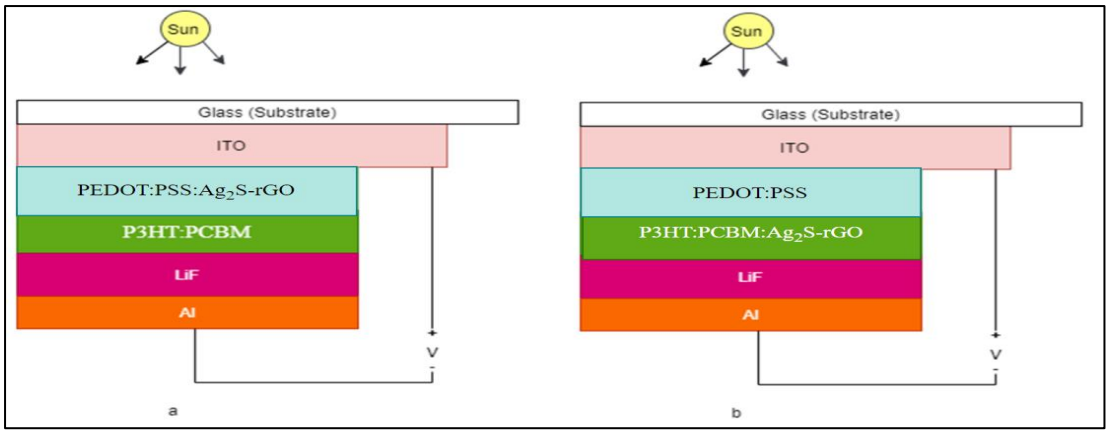

Figure 3.1: BHJ-OSC devices with modified: (a) HTL and (b) photoactive layer

3.5 Solar Cells Characterization

The transmission spectra of HTLs deposited on ITO and the absorption spectra of the photoactive layer of the solar cell were obtained using the UV-Vis spectrophotometer. The current density-voltage (*J-V*) characteristics of the fabricated solar cells were obtained from a source meter (Ossila Source Measure X-200) under a solar simulator (SCIENCETECH SciSun-150 class AAA), operating at AM 1.5 with an integrated power intensity of 100 mW/cm^2. The solar cell was mounted on the SourceMeter and then illuminated by the solar simulator. A solar simulator is a complete system with lenses, reflectors, shutters, control electronics, power supplies, and a high-intensity light source simulating the solar spectrum. The solar simulator illuminates the solar cell, and then the SourceMeter takes the readings of the parameters to be displayed on a PC, as shown in Figure 3.2.

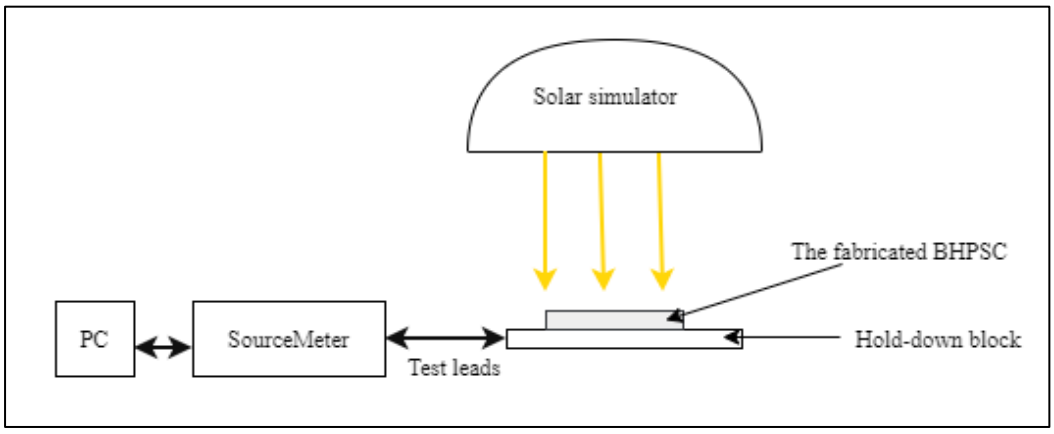

Figure 3.2: Configuration for measuring photovoltaic characteristics of the fabricated BHPSC

CHAPTER FOUR

RESULTS AND DISCUSSIONS

4.1 Morphological Properties of the Nanocomposite

The morphological characteristics of the Ag_2S-rGO nanocomposite synthesised were analysed with SEM, and the images obtained are presented in Figure 4.1 and Figure 4.2. Figure 4.1 shows Ag_2S in a nanowire shape. The nanowires of Ag_2S possess unique optoelectronic, electrical, and mechanical properties (Sadovnikov & Gusev, 2017). The optoelectronic properties of Ag_2S nanowires include high optical transmission and low sheet resistance, which resonates with the needs of OSCs (Khanarian et al., 2013; Sadovnikov & Gusev, 2017).

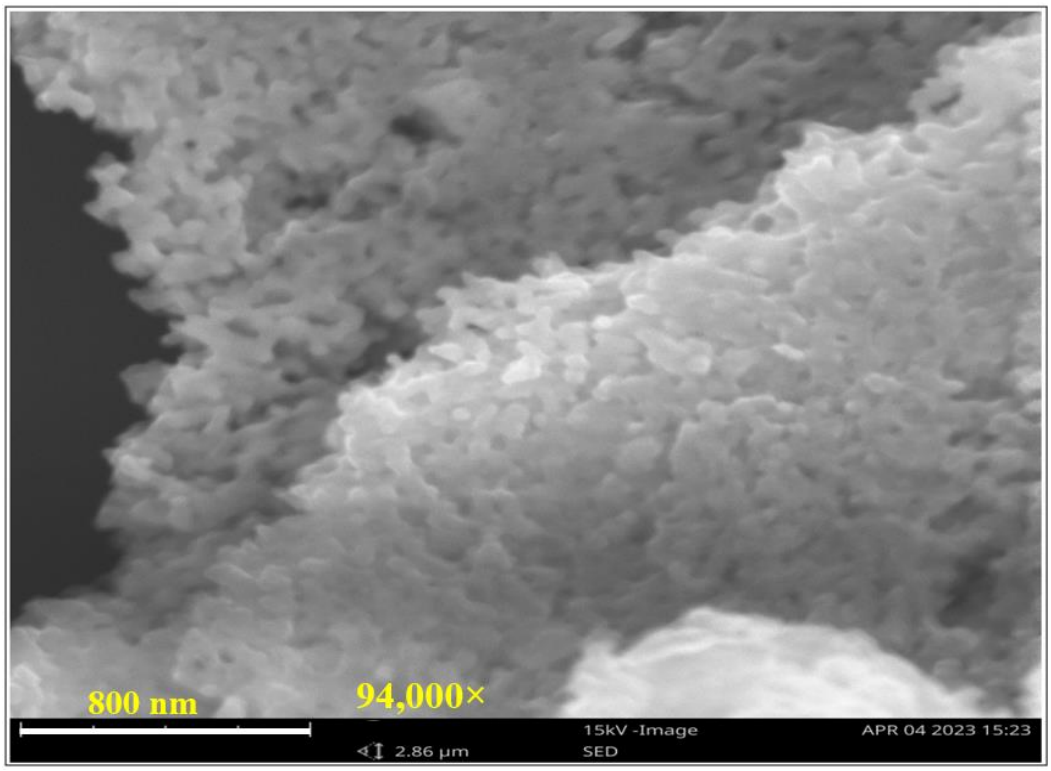

Figure 4.1: SEM image of Ag_2S-rGO with GO concentration of 150 mg

Figure 4.2 indicates a tightly packed structure of folded rGO. The observed structure resonates with Compton and Nguyen's (2010) demonstration that rGO possesses a tightly packed interlocking sheet structure. The importance of this structure is that rGO becomes uniformly distributed onto the surface of the Ag_2S, hence obtaining homogeneity in the synthesised nanocomposite. When GO gets chemically converted to graphene, defects and vacancies are introduced in the carbon structure (Pan et al., 2011). Homogeneity of the nanocomposite is achieved by having the crystals of Ag_2S grow around these vacancies and defect sites.

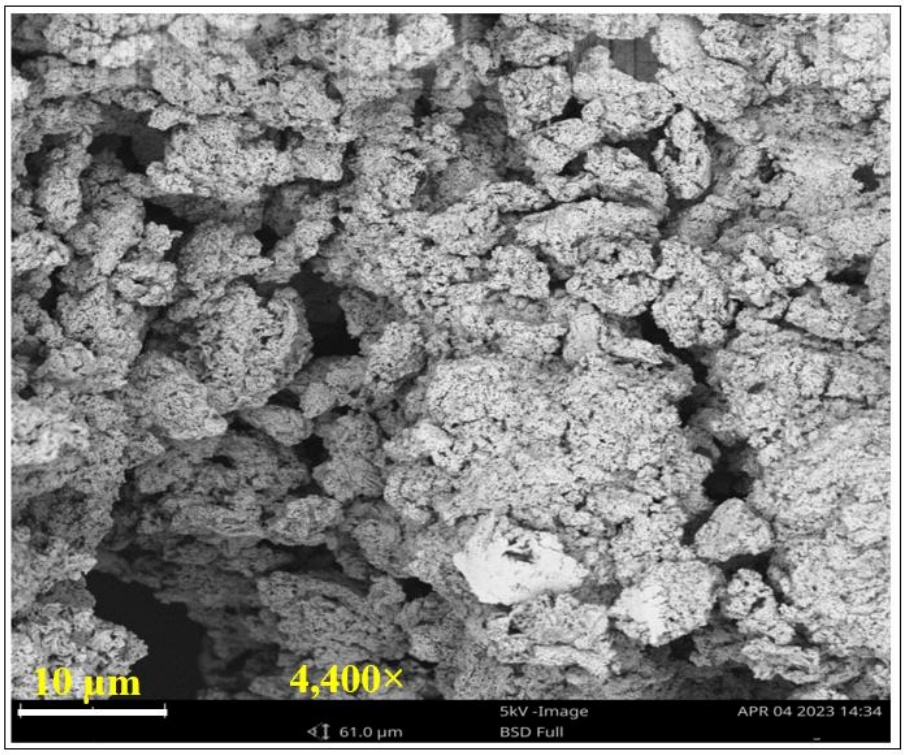

Figure 4.2: SEM image of Ag_2S-rGO with GO concentration of 10 mg

4.2 SEM-EDX Analysis

Figure 4.3 shows the spectrum of SEM-EDX elemental analysis of the Ag_2S-rGO nanocomposite. The Ag_2S-rGO nanocomposite consists of Ag_2S, which has silver (Ag) and sulphur (S), and rGO, which is composed of carbon (C) and oxygen (O). The SEM-EDX shows peaks for C, Ag, O, and S. The existence of the rGO in the nanocomposite is proved by the occurrence of C and O peaks in the spectrum. Only one O peak, with low intensity, was observed, showing a successful reduction of the GO in the synthesis process. The signals obtained in Figure 4.3 exhibit even distribution which means that the elements are well distributed throughout the rGO matrix rather than concentrated in one area (Naeem et al., 2023). Such a distribution of the elements indicates the nanocomposite's homogeneity. The

EDX elemental analysis confirms the purity of the nanocomposite since it does not show extra elemental signals in the material.

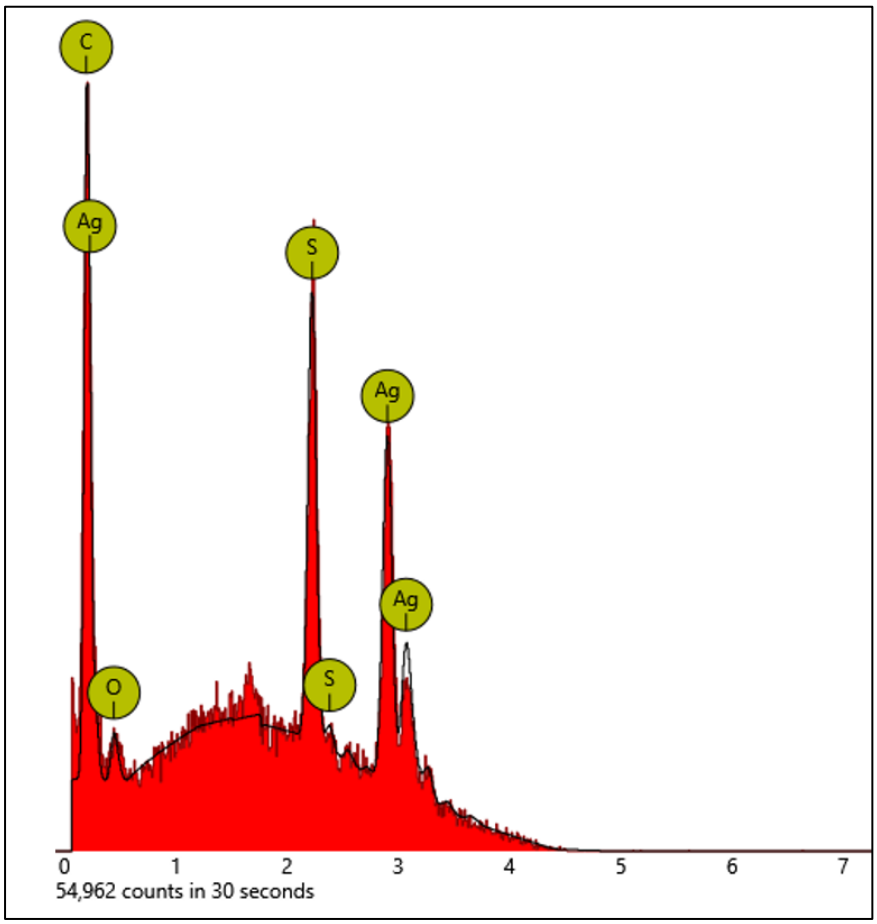

Figure 4.3: SEM-EDX Analysis of Ag_2S-rGO nanocomposite

4.3 Structural Properties of the Nanomaterials

Figure 4.4 shows the XRD spectrum for the Ag_2S NPs and Ag_2S-rGO nanocomposite. For Ag_2S NPs, the diffraction peaks were observed at 2θ values of 17.2°, 22.4°, 24.9°, 25.9°, 26.3, 28.9°, 31.5°, 33.6°, 34.38°, 34.7°, 36.8°, 37.7°, 40.7°, 43.4°, 46.2°, 47.8°, 48.7°, 53.2°, 58.3°, and 63.7° (Figure 4.4 a). These diffraction peaks correspond to the (011), (10-1), (110), (11-1), (022), (021), (111),(120), (120), (-121), (112), (013), (-113), (122), (210), (20-2), (113), (220), (221), and (-142) lattice planes of Ag_2S respectively, in the Joint Committee on Powder Diffraction Standards (JCPDS) card 96-900-0254 (Wiegers, 1971). These diffraction peaks indicate a monoclinic acanthite phase of Ag_2S NPs. The XRD analysis was done using Match! Software. The phase analysis resulting from the software also demonstrated that the synthesised

Ag_2S is a nanoparticle exhibiting a d-spacing of the diffraction lines ranging from 1.0 Å to 5.2 Å.

Figure 4.4 (b) shows additional XRD peaks of the nanocomposite at 2θ values of 26.3°, 44.3°, 54.2°, 83.2°, and 85.0° to the ones for Ag_2S NPs in Figure 4 (a) correspond to the (002), (101), (400), (112), and (006) crystalline planes of GO, respectively (JCPDS-card 01-075-1621). The dominant diffraction peak observed at 2θ = 26.3° corresponds to (002) of carbon with a d-spacing of 3.395 Å, which coincides with the (022) lattice plane of Ag_2S NPs, further demonstrating the uniformity of the nanocomposite formed (Moraes et al., 2015). The lack of XRD peaks below 12.0°, the GO characteristic diffraction peak, indicates the successful GO reduction during the chemical reduction process (Baskar et al., 2016; Moraes et al., 2015).

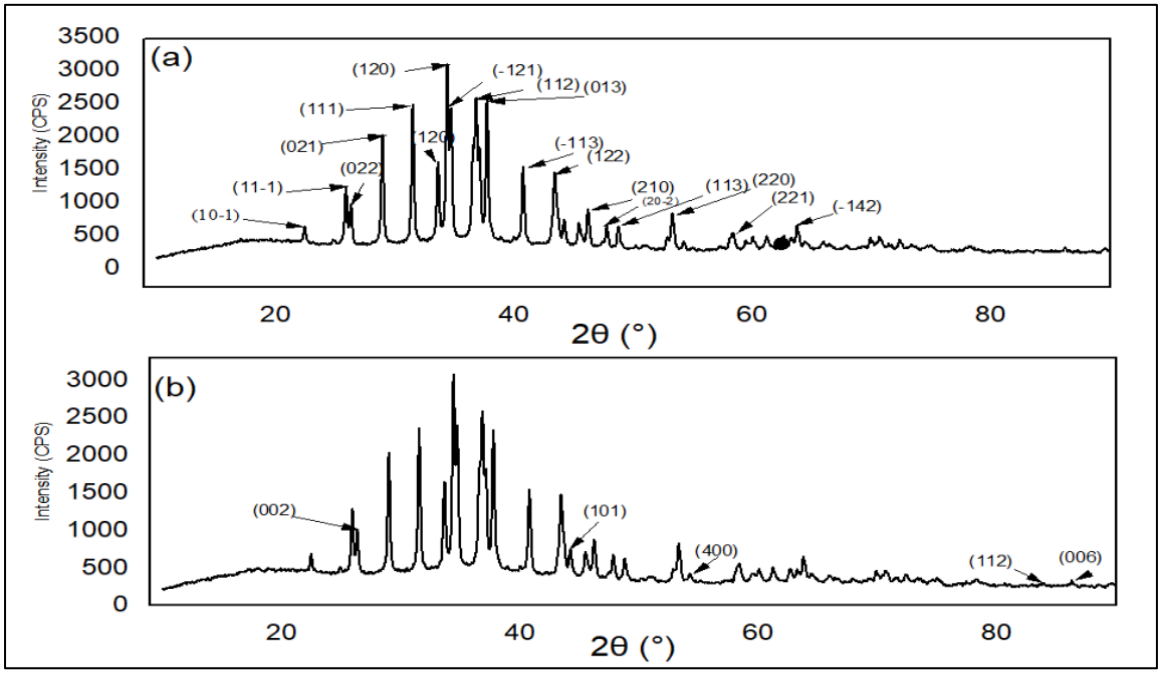

Figure 4.4: XRD patterns for (a) Ag_2S and (b) Ag_2S-rGO nanocomposite

4.4 Thermal Stability of the Nanomaterials

The results of the thermal stability analysis of the nanomaterials are seen in Figure 4.5. The TGA profiles of Ag_2S nanoparticles demonstrated a three-phase decomposition behaviour, as seen in Figure 4.5a. The weight loss was observed in the temperature ranges of 300°C to 480°C, 520°C to 700°C, and 760°C to 850°C.

The slight mass loss of Ag_2S from 300°C to 480°C is attributed to the desorption of the water molecules from the surface of the nanoparticles (Martínez et al., 2005). When Ag_2S nanoparticles get heated above the temperature of 175°C, there is a transition of acanthite to the argentite phase of the Ag_2S (Sadovnikov & Gusev, 2018). The region between 227°C and 527°C exhibits the argentite phase of Ag_2S (Sadovnikov & Gusev, 2018). This is the highest weight loss observed from 300°C to 480°C. Silver sulphide also exhibits other beta and gamma phases at higher temperatures. Above 160°C, Ag_2S exhibits β argentite phase, while above 587°C, it contains γ-Ag_2S phase (Sadovnikov & Gusev, 2018). Following the conversion of Ag_2S from β-Ag_2S to γ-Ag_2S between 627°C and 697°C, the coefficient of thermal expansion increases considerably (Sadovnikov & Gusev, 2018). It is inferred that this increased coefficient of thermal expansion is responsible for the steep weight loss from 520°C to 700°C. The last loss in weight from 760°C to 850°C is associated with the decomposition of the nanoparticles (Martínez et al., 2005).

The first observable weight loss of Ag_2S-rGO nanocomposite from the TGA occurred below 100°C and 210°C (Figure 4.5b). This weight loss is attributed to the decomposition of the functional oxygen groups in the nanocomposite (Moraes et al., 2015). The graphitic composition of the nanocomposite is expected to be completely decomposed by 600°C (Moraes et al., 2015). Thus, the remaining residue is of Ag_2S, which decomposes at a temperature of 981°C. The rGO constituent of the nanocomposite slowed the rate of decomposition between 520°C and 850°C; hence, the additions of rGO increase the nanocomposite's resistance to thermal degradation.

The derivative thermograms (DTG) of Ag_2S given in Figure 4.5c show three significant peaks at 180°C, 580°C, and 733°C. These peaks correspond to the Ag_2S phase transitions (Martínez et al., 2005). Specifically, the monoclinic acanthite of Ag_2S shows stability up to 176°C, after which the body-centred cubic argentite becomes stable between 176°C and 622°C; thereafter, there is a face-centred cubic polymorph (Martínez et al., 2005). This explains the irregular pattern in weight loss of Ag_2S at 713°C, in which there is an increase in weight, after which there is a fall from 766°C, as seen in Figure 4.5a.

As seen in Figure 4.5d, the DTG of Ag_2S-rGO shows peaks at 133 °C, 260 °C, 530 °C, and 845 °C. These peaks demonstrate the phase shifts of the nanocomposite. The peak at 845°C indicates the combustion of graphite (Farivar et al., 2021). The peak at 260 °C can be associated

with removing oxygen-containing groups from the nanocomposite (Tang et al., 2013). The endothermal peak observed at 133 °C indicates the decomposition of water molecules from the Ag_2S-rGO surface (Mahnashi et al., 2021). Since there is no other DTG peak characteristic of another element other than the main components of Ag_2S-rGO, the nanocomposite is considered pure.

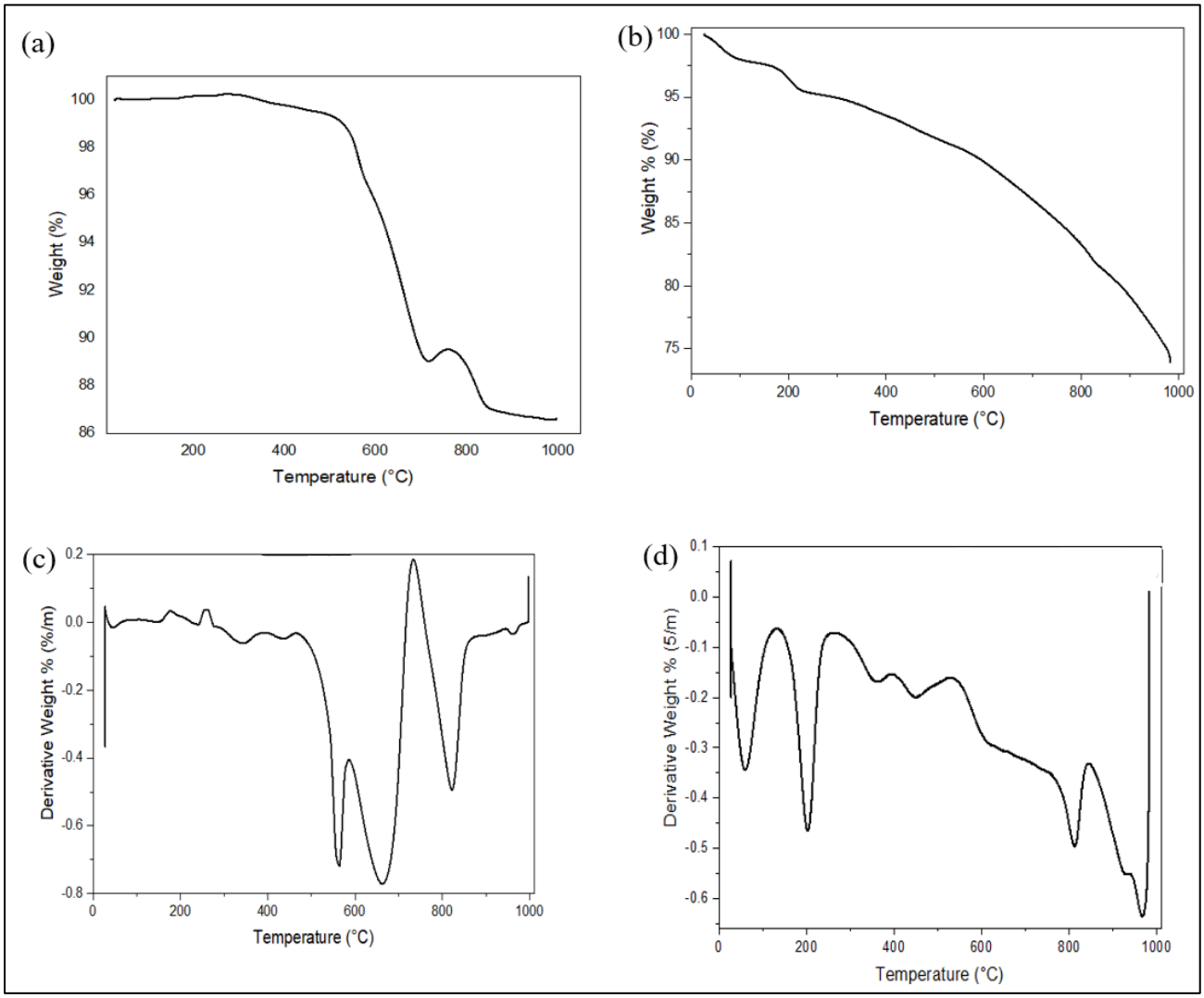

Figure 4.5: TGA thermograms of (a) Ag_2S and (b) Ag_2S-rGO; and derivative thermogram of (c) Ag_2S and (d) Ag_2S-rGO

4.5 Optical Absorption of the Nanomaterials

Figure 4.6 shows the UV-Vis spectra of Ag_2S NPs and Ag_2S-rGO nanocomposites. A common absorption peak appears at 202 nm for the Ag_2S nanoparticles and Ag_2S-rGO nanocomposite. For Ag_2S NPs, this peak is characteristic of the surface plasmon resonance of the nanowire-shaped nanoparticles (Delgado et al., 2018). Nanowire-shaped Ag_2S NPs, shown in Figure 4.1,

use LSPR to trap light effectively (Hamed et al., 2020). Figure 4.6b shows a peak at 202 nm, indicating superimposition of the absorbance of Ag_2S and rGO. The absorbance peak at 202 nm also demonstrates π-π* transitions of the C-C aromatic bonds for rGO (Ahmad et al., 2020; Gurunathan et al., 2015; Vi et al., 2018).

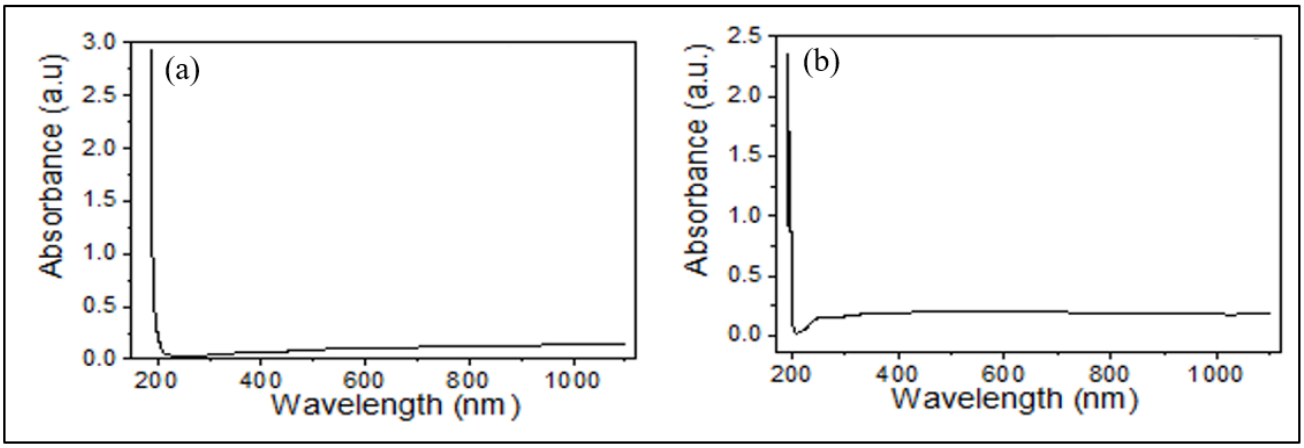

Figure 4.6: Optical absorption of (a) Ag_2S and (b) Ag_2S-rGO

4.6 FTIR Analysis of the Nanomaterials

The FT-IR was carried to identify the functional groups of the Ag_2S-rGO nanocomposite. Figure 4.7a shows the FT-IR spectrum of Ag_2S nanoparticles, while Figure 4.7b shows the spectrum for Ag_2S-rGO nanocomposite. For Ag_2S nanoparticles, the major bands were observed at 735 cm^{-1}, 1048 cm^{-1}, 1285 cm^{-1}, 1438 cm^{-1}, 1640 cm^{-1}, 2090 cm^{-1}, 2330 cm^{-1}, 2660 cm^{-1}, 2920 cm^{-1}, and 3840 cm^{-1}. The highest peaks in Ag_2S-rGO spectrum manifested at 630 cm^{-1}, 1055 cm^{-1}, 1290 cm^{-1}, 1320 cm^{-1}, 1420 cm^{-1}, 1640 cm^{-1}, 1995 cm^{-1}, 2100 cm^{-1}, 2340 cm^{-1}, 2680 cm^{-1}, 2855 cm^{-1}, 2920 cm^{-1}, 3747 cm^{-1}, and 3830 cm^{-1}.

The band at 3747 cm^{-1} for the nanocomposite indicates the presence of hydroxyl (OH) groups due to the addition of the rGO to the Ag_2S nanoparticles (Khalili, 2016; Khan et al., 2019). The band at 630 cm^{-1} in Figure 4.7b can be associated with the C-O-C and C-O bending vibrations (Khan et al., 2019). A common band appears at 1640 cm^{-1} for both Ag_2S and Ag_2S-rGO. The peak is resonant with the elongation and flexion of OH groups of water molecules (Khan et al., 2019; Zhao et al., 2020). A band is observed to emerge at 630 cm^{-1} in the Ag_2S-rGO nanocomposite. This occurrence can be explained by the chelation of blank orbits in Ag_2S, which are deficient in electrons to the atoms in O-H, rich in O, and the sp^2-conjugated bonds

on the rGO surface (Molla et al., 2019). The IR spectrum indicates a high interaction of the Ag_2S and the matrix of rGO, confirming the immobility of Ag_2S on the GO matrix's surface.

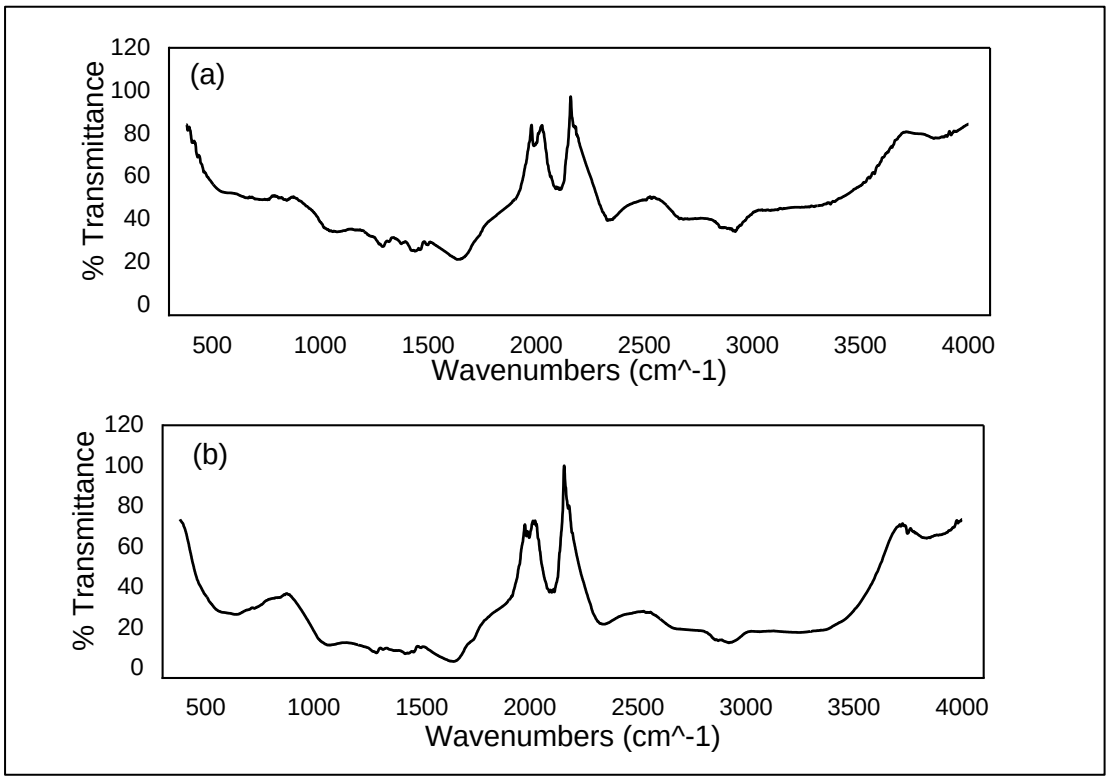

Figure 4.7: FTIR spectra of (a) Ag_2S and (b) Ag_2S-rGO

4.7 Optical Characterization of the Solar Cells

4.7.1 Optical Absorption of the Active Layer

The optical absorption of the photoactive layer of the devices was investigated. The acceptor material of the photoactive layer, PCBM, is known to have low light absorption, causing low efficiency of the OSCs (Manzano et al., 2015). The charger carriers should be photogenerated with high efficiency, which requires high light absorption in the photoactive layer (Amollo et al., 2018a). Figure 4.8 shows the UV-Vis absorbance spectra for the photoactive layers of P3HT: PCBM with Ag_2S-rGO nanocomposite added at varied concentrations of (a) 10 wt% and (b) 30 wt%. From this section, the nanocomposites prepared with GO concentrations of 100 mg in 100 ml of distilled water and 150 mg in 150 ml of distilled water will be referred to as Ag_2S-rGO-1 and Ag_2S-rGO-2, respectively.

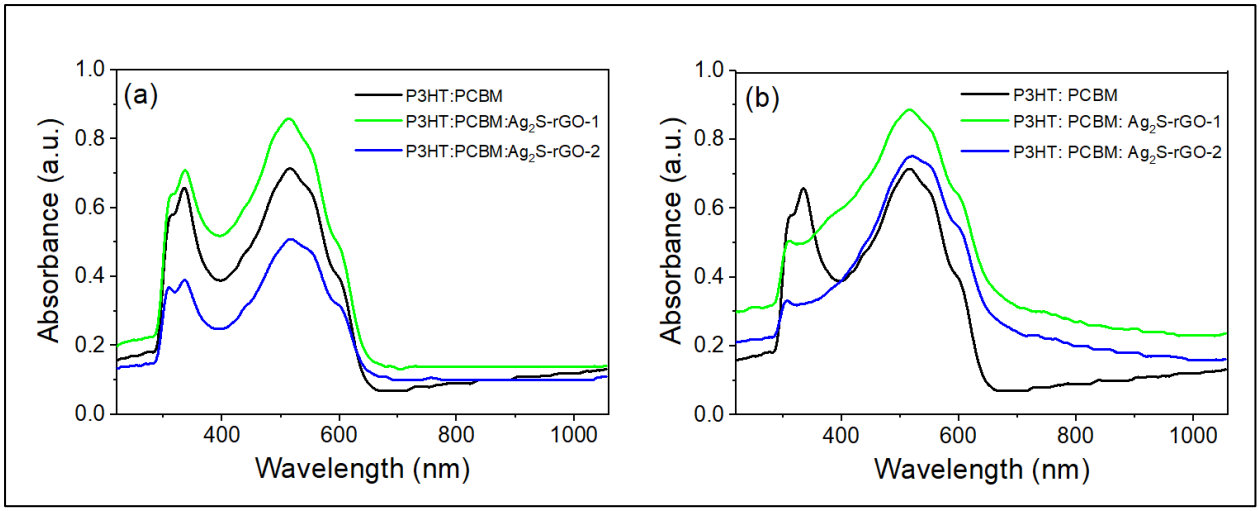

Figure 4.8: Optical absorption spectra for P3HT: PCBM photoactive layers with (a) 10 wt% and (b) 30 wt% loadings of Ag_2S-rGO

At 10 wt.%, the photoactive layer with Ag_2S-rGO-1 demonstrated the strongest absorption compared to the pure P3HT: PCBM and Ag_2S-rGO-2 in the visible region. Active layers with Ag_2S-rGO-1 and Ag_2S-rGO-2 at 30 wt.% loadings show higher absorption within the visible region than the non-modified devices (Figure 4.8b).

The observed stronger absorption peaks of the active layers with Ag_2S-rGO-1 at 10 and 30 wt.% and Ag_2S-rGO-2 at 30 wt.% compared to P3HT: PCBM can be attributed to the contribution of rGO and Ag_2S NPs in the nanocomposite. At optimal concentration, rGO minimises the torsional disorders of the P3HT chains, thereby causing an increase in its conjugational length (Bkakri et al., 2015). This implies increased alterations of the single-double bonds within the chains of the polymer (Ismail et al., 2015), which leads to improved absorption of photons and increases the charge generation in OSCs. The nanocomposite also enhances the absorption peaks of the P3HT: PCBM in the UV regions due to the presence of Ag_2S NPs in the nanocomposite (Hamed et al., 2020). It is observed from Figure 4.8 that films with Ag_2S-rGO-1 at 10 wt.% have higher absorption peaks at 338 nm and 515 nm, and Ag_2S-rGO-2 at 30 wt.% have high absorbance peaks at 515 nm. The peaks within the UV region are contributed to by the surface plasmon polarisation resonance characteristic of collective oscillation of conductive electrons on the Ag_2S surface (Hamed et al., 2020). However, the peaks in the visible regions can be related to the contribution from the surface distribution of Ag_2S sizes that increases the surface scattering and states (Hamed et al., 2020). The absorption peak in the visible region is more intense than the one in the UV region, showing that Ag_2S

gets more activated in the visible than in the UV region, thereby enhancing the light absorption (Cui et al., 2015). The lower absorption of the active layers with Ag_2S-rGO-2 at 10 wt.% than the reference device can be explained by the possibilities of agglomeration of the graphene layers in the nanocomposite, since Ag_2S-rGO-2 has a higher rGO concentration than Ag_2S-rGO-1 at 10 wt.%. This implies that the contribution of Ag_2S on light trapping through LSPR is negligible. The clumping of the sheets of graphene in the device reduces the P3HT lamellae degree of order, reducing the devices' optical absorption (Bkakri et al., 2015). Hence, inclusion of Ag_2S-rGO to OSCs' photoactive layer at optimum concentration leads to an increase in light absorption depending on the concentration of rGO in the nanocomposite and the overall weight loading of the nanocomposite to the polymer matrix.

The addition of the nanocomposite in the active layer causes a slight expansion of the bandwidth of the material to absorb light. Figure 4.8b shows that at 30 wt.% loadings, all the modified devices with all the concentrations of rGO in the nanocomposite showed a lower absorption onset at about 332 nm compared to the reference device, which starts at 395 nm. Similar trends have been reported in the work by Amollo et al. (2018a). The broadening of the absorption spectrum is attributed to the Ag_2S-rGO nanocomposite contribution to the active material's polymer matrix. The slightly broadened absorption spectrum implies that the donor polymer has a lowered bandgap (Amollo et al., 2020b). A lowered bandgap means broadened absorption bands, hence better performance of the solar cells. Nanocomposites with Ag_2S NPs as one of their components have shown improved spectrum utilisation (Kumar et al., 2019).

4.7.2 Optical Transmittance of the HTL

Figure 4.9 shows the optical transmittance spectra of PEDOT:PSS:Ag_2S-rGO coated on an ITO substrate. At 20 wt.% loading of the nanocomposite, the reference, and the PEDOT:PSS: Ag_2S-rGO-1 showed the highest transmittance of 100% at 327 nm (Figure 4.9a). The expectation is that the incorporation of Ag_2S-rGO-1 and Ag_2S-rGO-2 at 20 wt.% and 30 wt.% to the PEDOT: PSS HTL will not adversely affect the light transmittance and absorption in the HTL and the photoactive layer, respectively, within the UV region, but slightly lower the transmittance in the visible region. At 20 wt.%, PEDOT:PSS:Ag_2S-rGO-2 had a lower optical transmittance of 94% at the wavelength of approximately 327 nm compared to the reference and PEDOT:PSS:Ag_2S-rGO-1 HTLs. At 30 wt.% (Figure 4.9b), all the modified HTLs had a lower transmittance than the reference HTL in both the UV and the visible regions. Transmittance of

the modified HTL has been reduced due to the enhanced absorption of incident light by the nanocomposite. Silver nanoparticles are known to trap light through LSPR, which could have contributed to the absorption of some light in the modified HTL (Hamed et al., 2020). The rGO in the nanocomposite also has high optical absorbance, lowering the transmittance of the modified HTL (Amollo et al., 2018a). The strong absorbance of rGO also explains why the modified HTL exhibited lower transmittance in the visible region with the increase in the concentration of rGO in the nanocomposite for both the 20 wt.% and 30 wt.% loadings of the nanocomposite.

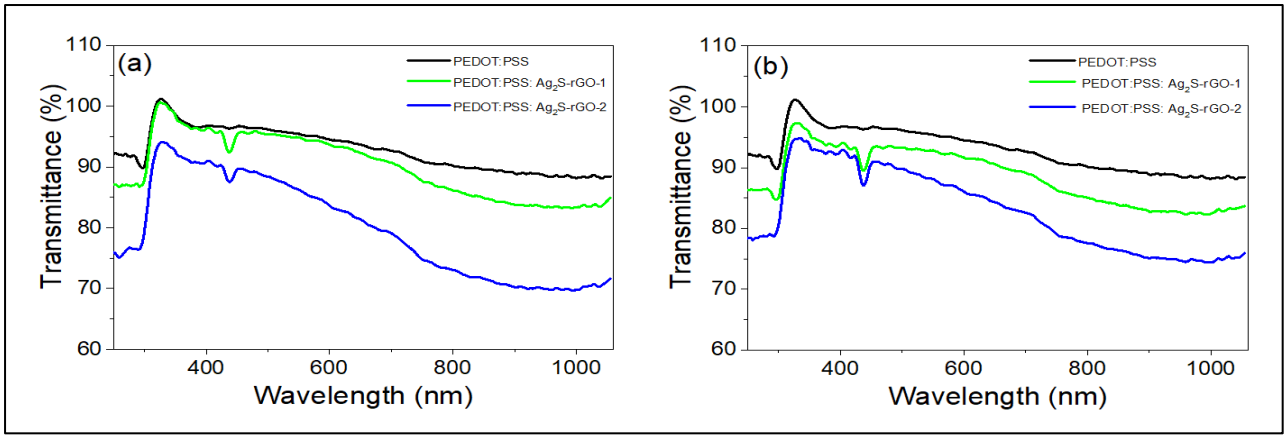

Figure 4.9: Optical transmission spectra of PEDOT: PSS HTL with (a) 20 wt% and (b) 30 wt% loadings of Ag_2S-rGO

The modified HTLs have a dip in transmittance at about 435 nm for both 20 wt.% and 30 wt.% loadings, which the reference HTL does not have. This reduction in transmittance is explained by the dipole plasmon resonance of the silver nanoparticles, which absorb the light in the region of 435 nm (Ahmad et al., 2020). In BHJ, both the active layer and HTL compete for light harvesting, implying that the optical properties of the latter will influence those of the former (Hou et al., 2015). However, only the absorbed light in the photoactive layer will help generate excitons in the BHJ devices.

4.8 Photovoltaic Characterization of Solar Cells

4.8.1 HTL Modification

All the devices with the nanocomposite in the HTL demonstrated a significant improvement in their photovoltaic performances, as seen in Table 4.1. Figure 4.10 shows the *J-V* characteristics of the devices having modified HTL. As seen in Table 4.1, the PCE, FF, and J_{sc} improved with

the increase in the concentration of rGO in the nanocomposite at 20 wt.% loading of the nanocomposite to the HTL material. The introduction of the Ag_2S-rGO to the HTL caused a higher current density, which enhanced the device's performance (Amollo et al., 2018b). A study by Rivera-Taco et al. (2021) showed that introducing silver nanoparticles into PEDOT: PSS in OSCs increased the J_{SC} from 10 mA cm^{-1} to 11.0 mA cm^{-1}, improving the PCE to 2.0% from 1.7%. In their research, the nanocomposite augmented the interfacial surface area between the HTL and the active layer (Rivera-Taco et al., 2021). Therefore, the increased interfacial area implies an improved efficiency of hole collection at the anode, further improving the J_{SC} of the OSC devices. Doping PEDOT: PSS with silver nanoparticles increased its electrical conductivity from 0.5 Scm^{-1} to 200 Scm^{-1} (Rivera-Taco et al., 2021). This improvement in the device performance of the modified HTL device shows the importance of the Ag_2S-rGO nanocomposite in enhancing a better charge extraction at the photoactive layer-HTL junction.

The PCE and J_{SC} of the HTL-modified devices, however, reduced with the rise in the rGO concentration in the nanocomposite at 30 wt.% loading of the nanocomposite. Although the PCE for the devices with Ag_2S-rGO-1 and Ag_2S-rGO-2 nanocomposites, at 30 wt.% loadings, in the HTL are higher than for the pristine PEDOT: PSS HTL devices, Ag_2S-rGO-2 demonstrated less PCE, FF, Voc, and J_{SC} compared to the devices with Ag_2S-rGO-1 (Table 1). The best-performing device with modified HTL was demonstrated to be the one with Ag_2S-rGO-1 nanocomposite at 30 wt.% loadings, while the lowest-performing device had Ag_2S-rGO-2 at 30 wt.% loading in the HTL. The poorer performance of the devices having Ag_2S-rGO-2 in the HTL can be explained by increased recombination of the charge carriers in the device (Amollo et al., 2018b). The higher loss in charger carriers is also observed from the higher R_S for devices with Ag_2S-rGO-2 in HTL compared to those with Ag_2S-rGO-1.

Table 4.1: Photovoltaic parameters of modified HTL with different loadings of Ag_2S-rGO

Nanocomposite Concentration (wt.%)	**HTL Material**	**PCE (%)**	**FF (%)**	J_{SC} **(mA** cm^{-2}**)**	V_{OC} **(volts)**	R_s **(Ω)**
Reference	PEDOT: PSS	1.5	41	6.9	0.55	152
20	PEDOT: PSS: Ag_2S-rGO-1	1.9	31	11	0.55	34
	PEDOT: PSS: Ag_2S-rGO-2	2.0	32	12	0.54	30
30	PEDOT: PSS: Ag_2S-rGO-1	2.3	35	12	0.53	20
	PEDOT: PSS: Ag_2S-rGO-2	1.7	33	10	0.50	25

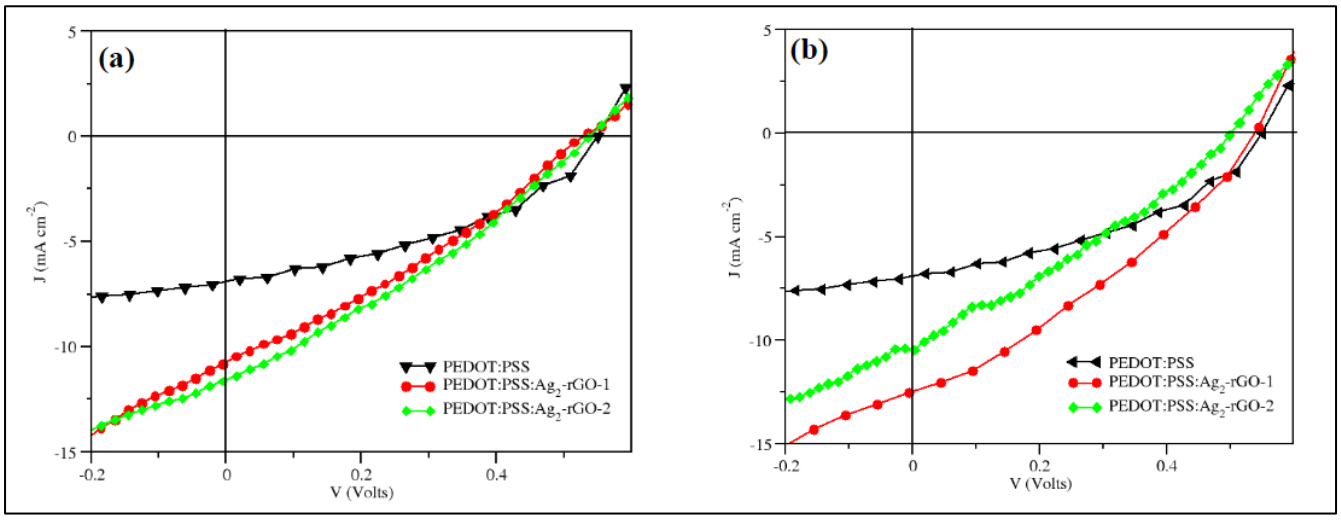

Figure 10.10: The *J-V* characteristics of the PEDOT: PSS HTL with (a) 20 wt.% and (b) 30 wt.% loadings of Ag_2S-rGO

As the concentration of rGO increases in the nanocomposite and thus the device, agglomeration of the nanocomposite occurs, which impedes the movement of charges to the anode (Amollo et al., 2020b). The performance of the device with Ag_2S-rGO-2 in the HTL is still better than that of the reference device since rGO has been reported to form a low-injection barrier between the HTL and the donor material (Li et al., 2010b). The created low injection barrier allows for easy injection of holes at the HTL and collection at the anode.

4.8.2 Photoactive Layer Modification

The solar cells with different photovoltaic parameters with different nanocomposite loadings of 10, 20, and 30 wt.% into the photoactive layer material are recorded in Table 4.2. Figure 4.11 shows the plots of the *J-V* characteristics of the devices. The findings reveal that all the devices with modified photoactive layers performed better than the reference devices. All the devices with Ag_2S-rGO added to the photoactive layer exhibited enhanced J_{sc} and PCE. The enhanced J_{sc} is associated with improved charge generation, collection, and transport due to incorporating the nanocomposite into the photoactive layer (Amollo et al., 2020b). Because of the enhanced J_{sc}, the PCE also substantially improved after incorporating the nanocomposite into the photoactive layer of the devices.

Table 4.2: Photovoltaic parameters of the modified photoactive layers at different loadings of Ag_2S-rGO

Nanocomposite Concentration (wt.%)	Active Layer Material	PCE (%)	FF (%)	J_{SC} (mA cm^{-2})	V_{OC} (volts)	R_s (Ω)
Reference	P3HT: PCBM	1.5	41	6.9	0.55	152
10	P3HT: PCBM: Ag_2S-rGO-1	2.5	30	9.9	0.51	46
	P3HT: PCBM: Ag_2S-rGO-2	2.6	34	15	0.52	24
20	P3HT: PCBM: Ag_2S-rGO-1	2.8	27	11	0.55	41
	P3HT: PCBM: Ag_2S-rGO-2	2.5	32	14	0.54	18
30	P3HT: PCBM: Ag_2S-rGO-1	3.4	33	17	0.59	22
	P3HT: PCBM: Ag_2S-rGO-2	2.1	31	12	0.57	29

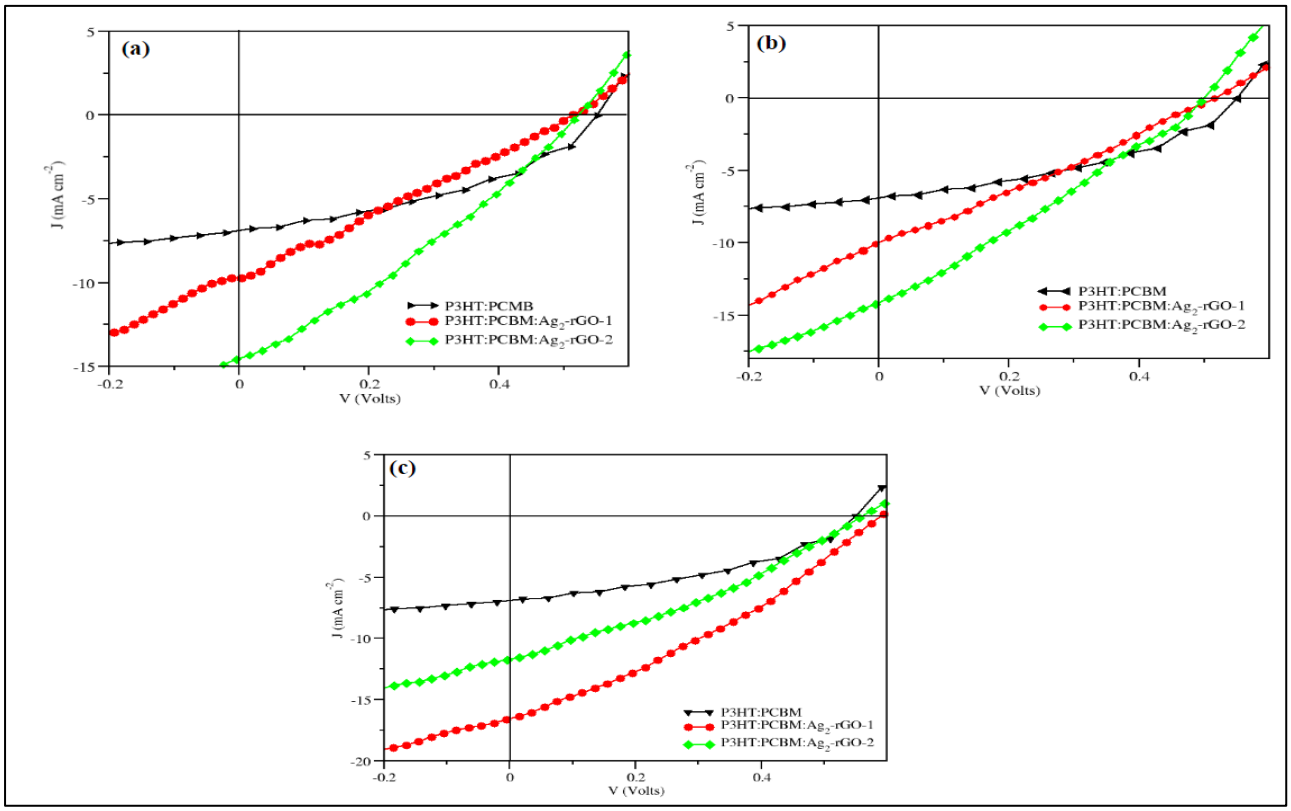

Figure 4.11: The J-V characteristics of the P3HT: PCBM photoactive layer with (a) 10 wt.%, (b) 20 wt.%, and (c) 30 wt.% loadings of Ag_2S-rGO

The enhanced performance of the solar cells, as seen in Figure 4.11, can be explained by the strong optical absorbance of modified solar cell devices with Ag_2S-rGO-1 at 10 wt.% and Ag_2S-rGO-1 and Ag_2S-rGO-2 at 30 wt.%. In addition to the effective generation of excitons,

their optimal dissociation and transportation to the electrodes determine the performance of OSCs (Amollo et al., 2018a). Although devices with Ag_2S-rGO-2 at 10 wt.% had lower absorbance than the reference device within the visible region (Figure 4.8a), they still had higher performance than the reference solar cell. The implication is that there will be improved charge separation and movement in the devices.

Even though adding the Ag_2S-rGO-2 nanocomposite to the photoactive layer improves the solar cells' PCE, FF, and J_{SC}, as indicated in Table 4.2, the efficiency slightly decreases as the wt.% loading increases. The PCE (and FF) of the solar cells with Ag_2S-rGO-2 in the photoactive layer decreases from 2.6% (34) to 2.5% (32) and 2.1% (31) for 10, 20, and 30 wt.% loadings, respectively. This declining performance can be associated with the possibility of the Ag_2S-rGO nanocomposite forming agglomerates on the active layer film; the agglomerates act as charge traps to cause charge carrier loss. On the contrary, the PCE of the devices with Ag_2S-rGO-1 increased with the increase in wt.% loading in the photoactive layer. The PCE increased from 2.5% for 10 wt. % loading to 2.8% for 20 wt.% loading and 3.4% for 30 wt.% loadings, respectively.

Table 4.2 shows that the FF for devices with Ag_2S-rGO-1 in the photoactive layer at 20 wt.% is relatively lower than for the device with pristine P3HT: PCBM as the photoactive layer material. Such a lower FF indicates the possibility of short-circuit pathway current leakages (Amollo et al., 2020b). These current leakages occur in local defect states. A possible source of losses in charge carriers is the imbalance in the mobility of the carriers within the bulk blend of the photoactive layer (Smith et al., 2014). Therefore, the improved PCE of the devices with modified photoactive layers is caused by the increase in the absorption of light, as demonstrated in Figure 4.8b (where devices with Ag_2S-rGO-1 demonstrate the highest optical absorbance compared to Ag_2S-rGO-2 and reference devices) and a subsequent photogeneration of charge carriers, indicated by improved J_{sc}.

CHAPTER FIVE

SUMMARY, CONCLUSIONS AND RECOMMENDATIONS

5.1 Summary

The problem of global climate change and economic growth has prompted an increase in demand for clean energy to supplement the currently used fossil fuels, which are almost depleted, besides are a significant contributor to climate change. Reliability and cost are common challenges in determining the most appropriate alternative clean energy source. Solar energy is one of the clean sources of energy that is cost-effective, but its power conversion efficiencies are low, specifically, OSCs. The research demonstrated the impact of Ag_2S-rGO on the performance of OSCs when used in the photoactive layer and the HTL, where all modified solar cell devices had improved performance. The chemical reduction method was used to synthesise Ag_2S-rGO nanocomposite with high crystallinity.

The SEM images of the nanocomposite showed that rGO sheets were intercalated in Ag_2S nanoparticles during the chemical reduction method. The SEM analysis also showed that Ag_2S had the shape of nanowires. The TGA analysis of the Ag_2S-rGO nanocomposite showed a significant weight loss at 157°C to 211°C, indicating the decomposition of the oxygenated functional groups. The TGA further showed that rGO enhances the thermal stability of nanocomposite. The DTG analysis of the nanocomposite showed endothermic peaks at 133°C, 260°C, 530°C, and 845°C demonstrating the phase shifts of the nanocomposite with a DTG peak at 845°C showing the combustion of graphite. The lack of DTG and EDX peaks for elements other than those in the Ag_2S-rGO showed the purity of the nanocomposite.

The d-spacing for the diffraction lines in XRD ranged between 1.0 Å and 5.2 Å, indicating that the composite formed was in nanoscale. The presence of rGO in the nanocomposite was confirmed by a strong XRD peak at The XRD 2θ = 26.3°, corresponding to the miller index (002) of carbon. The nanocomposite exhibited strong absorbance within the UV and visible regions. The FT-IR spectrum of the nanocomposite showed a band at 3747 cm^{-1} indicating the presence of hydroxyl (OH) groups. A common band appeared in 1640 cm^{-1} for both Ag_2S and Ag_2S-rGO. The FT-IR depicted a strong interaction between Ag_2S and the matrix of rGO. The nanocomposite is easily dispersed in polar and non-polar solvents, making it applicable in OSCs.

The UV-Vis analysis of the fabricated devices with the Ag_2S-rGO in the photoactive layer demonstrated a strong absorbance within the UV region. For the optical transmittance of the HTL-modified devices, the UV-Vis spectra showed that at 20 wt.% loading of the nanocomposite, the reference, and the PEDOT: PSS: Ag_2S-rGO-1 showed the highest transmittance of 100% at 327 nm, indicating that adding a nanocomposite or rGO to PEDOT: PSS does not interfere with the optical transmittance of the polymer. The PEDOT: PSS: Ag_2S-rGO-2, however, demonstrated a lower optical absorbance at 20 wt.% loading compared to the reference and PEDOT: PSS: Ag_2S-rGO-1 HTLs. All the HTL-modified devices demonstrated lower transmittance at 30 wt.%. The devices with modified photoactive layers performed better than the reference devices due to improved charge generation and collection. The solar cell efficiency decreased with the increase in wt.% loading of Ag_2S-rGO-2 to the photoactive layer due to the possibility of agglomeration of the nanocomposite. Devices with the nanocomposite in the HTL demonstrated considerable performance improvement, with the PCE increasing with the increase in the concentration of rGO in the nanocomposite at 20 wt.% loading. However, due to increased charge carrier loss, the HTL-modified devices' performance decreased with the increase of rGO in the nanocomposite for 30 wt.%. The findings of this research indicate that the application of Ag_2S-rGO nanocomposite to the photoactive layer and HTL of the OSCs considerably improves the solar cell's performance.

5.2 Conclusions

i. The chemical reduction method was successful in synthesising Ag_2S-rGO nanocomposite, demonstrated by the nanowire shape of Ag_2S nanoparticles intercalated with rGO sheets and the nanocomposite demonstrating high crystallinity.

ii. The characterization of Ag_2S-rGO nanocomposite confirmed nanoscale features of the nanocomposite (XRD), nanowire morphology (SEM), high thermal stability with the integration of rGO in the nanocomposite (TGA and DTG), strong absorbance in the UV and visible regions (UV-Vis), and presence of functional groups (FTIR) indicating purity and stability of the nanomaterials.

iii. All devices with Ag_2S-rGO nanocomposite in the photoactive and hole transport layers of the OSCs demonstrated enhanced light absorption, PCE, and mobility of charge carriers, though at non-optimal concentrations of rGO, there was a slight decline in performance due to agglomeration of rGO.

5.3 Recommendations

i. It is recommended to explore other methods for synthesising Ag_2S-rGO nanocomposites, such as hydrothermal and solvothermal methods, since they help in controlling morphology, particle size of Ag_2S, and distribution on the rGO matrix.

ii. Optimise the concentration of Ag_2S in the nanocomposite. It is recommended to have rGO constant and vary the concentration of Ag_2S in the nanocomposite. Since Ag_2S has a narrow bandgap of between 0.9 eV and 1.05 eV, varying its concentration in the nanocomposite for the HTL would be interesting in monitoring the PCE of the OSCs due to the impact of the nanoparticle on the charge carrier mobility. It would also be interesting to monitor the effect of the Ag_2S-rGO nanocomposite in the active layer of OSCs with varying concentrations of Ag_2S in the nanocomposite.

iii. Simultaneously modify both the photoactive and HTL layers. The study investigated the impact of Ag_2S-rGO nanocomposite when applied to either the HTL or photoactive layer of the OSC. Since the modification of the HTL and the active layer demonstrated improvement, applying the nanocomposite to both the HTL and the active layers of the OSCs simultaneously to monitor the impact on the performance of the solar cell would be necessary.

5.4 Suggestion for Further Research

Further research is recommended to investigate the performance of OSCs when the Ag_2S-rGO nanocomposite is simultaneously applied to both the HTL and photoactive layer of the solar cells. Additionally, it is appropriate to investigate the changes in the OSC's performance with varying concentration of Ag_2S in the Ag_2S-rGO nanocomposite.

REFERENCES

Agnihotri, P., Sahu, S., & Tiwari, S. (2017). Recent advances & perspectives in electron transport layer of organic solar cells for efficient solar energy harvesting. *2017 International Conference on Energy, Communication, Data Analytics and Soft Computing (ICECDS)*, 1568–1573. https://doi.org/10.1109/ICECDS.2017.8389710

Ahmad, H., Albaqawi, H. S., Yusoff, N., Reduan, S. A., & Yi, C. W. (2020). Reduced graphene oxide-silver nanoparticles for optical pulse generation in ytterbium- and erbium-doped fiber lasers. *Scientific Reports*, *10*(1), 1–11. https://doi.org/10.1038/s41598-020-66253-w

Akter, N., Paul, P. S., Mondal, S., & Mominuzzaman, S. M. (2014). Modeling and analysis of inorganic, organic, and hybrid solar cells. *8th International Conference on Electrical and Computer Engineering*, 520–523. https://doi.org/10.1109/ICECE.2014.7026911

Amollo, T. A., Mola, G. T., & Nyamori, V. O. (2017). Reduced graphene oxide-germanium quantum dot nanocomposite: electronic, optical, and magnetic properties. *Nanotechnology*, *28*(49), 495703. https://doi.org/10.1088/1361-6528/aa9299

Amollo, T. A., Mola, G. T., & Nyamori, V. O. (2018a). High-performance organic solar cells utilizing graphene oxide in the active and hole transport layers. *Solar Energy*, *171*(5), 83–91. https://doi.org/10.1016/j.solener.2018.06.068

Amollo, T. A., Mola, G. T., & Nyamori, V. O. (2018b). Polymer solar cells with reduced graphene oxide–germanium quantum dots nanocomposite in the hole transport layer. *Journal of Materials Science: Materials in Electronics*, *29*(9), 7820–7831. https://doi.org/10.1007/s10854-018-8781-1

Amollo, T. A., Mola, G. T., & Nyamori, V. O. (2020a). Organic solar cells: Materials and prospects of graphene for active and interfacial layers. *Critical Reviews in Solid State and Materials Sciences*, *45*(4), 261–288. https://doi.org/10.1080/10408436.2019.1632791

Amollo, T. A., Mola, G. T., & Nyamori, V. O. (2020b). Improved short-circuit current density in bulk heterojunction solar cells with reduced graphene oxide-germanium dioxide nanocomposite in the photoactive layer. *Materials Chemistry and Physics*, *254*, 1–24. https://doi.org/10.1016/j.matchemphys.2020.123448

Anagnostou, K., Stylianakis, M. M., Petridis, K., & Kymakis, E. (2019). Building an organic solar cell: fundamental procedures for device fabrication. *Energies*, *12*(11), 2188. https://doi.org/10.3390/en12112188

Arabpour, F., Ahmadi, N., Ahmadi, V., Di Carlo, A., Oniy Aghmiuni, K., Shokrolahzadeh Tehrani, A., Ghoreishi, F. S., Payandeh, M., & Mansour Rezaei Fumani, N. (2018). Bulk

heterojunction polymer solar cell and perovskite solar cell: Concepts, materials, current status, and optoelectronic properties. *Solar Energy*, *173*, 407–424. https://doi.org/10.1016/j.solener.2018.07.058

Bahrami, Z., Salehi, A., & Eyvaraghi, A. M. (2019). AMPS-1D Modelling of P3HT/PCBM bilayer and BHJ organic solar cell. *2019 27th Iranian Conference on Electrical Engineering (ICEE)*, 41–45. https://doi.org/10.1109/IranianCEE.2019.8786641

Baskar, S., Lavanya, T., Subramani, K., & Satheesh, K. (2016). Synthesis and characterization of reduced graphene oxide/Ag_2S nanocomposites by co-precipitation method using thiourea as sulfur source and reducing agent. *International Journal of ChemTech Research*, *9*(5), 395–401.

Bezrukikh, P. P., Karabanov, S. M., & Bezrukikh, P. P. (2016). Renewable energy efficiency. *2016 IEEE 16th International Conference on Environment and Electrical Engineering (EEEIC)*, 1–5. https://doi.org/10.1109/EEEIC.2016.7555545

Bkakri, R., Chehata, N., Ltaief, A., Kusmartseva, O. E., Kusmartsev, F. V., Song, M., & Bouazizi, A. (2015). Effects of the graphene content on the conversion efficiency of P3HT: Graphene-based organic solar cells. *Journal of Physics and Chemistry of Solids*, *85*, 206–211. https://doi.org/10.1016/j.jpcs.2015.05.020

Braun, A., Katz, E. A., Schwarzburg, K., Hannappel, T., & Gordon, J. M. (2012). Irradiance-dependent current-limiting behavior of multijunction solar cells. *2012 38th IEEE Photovoltaic Specialists Conference*, 001246–001249. https://doi.org/10.1109/PVSC.2012.6317828

Brédas, J.-L., Norton, J. E., Cornil, J., & Coropceanu, V. (2009). Molecular understanding of organic solar cells: the challenges. *Accounts of Chemical Research*, *42*(11), 1691–1699. https://doi.org/10.1021/ar900099h

Carley, S., & Konisky, D. M. (2020). The justice and equity implications of the clean energy transition. *Nature Energy*, *5*(8), 569–577. https://doi.org/10.1038/s41560-020-0641-6

Chanchangi, Y. N., Ghosh, A., Baig, H., Sundaram, S., & Mallick, T. K. (2021). Soiling on PV performance influenced by weather parameters in Northern Nigeria. *Renewable Energy*, *180*, 874–892. https://doi.org/10.1016/j.renene.2021.08.090

Cheng, P., Li, G., Zhan, X., & Yang, Y. (2018). Next-generation organic photovoltaics based on non-fullerene acceptors. *Nature Photonics*, *12*(3), 131–142. https://doi.org/10.1038/s41566-018-0104-9

Choudhury, S. A., & Chowdhury, M. H. (2016). Use of plasmonic metal nanoparticles to

increase the light absorption efficiency of thin-film solar cells. *2016 IEEE International Conference on Sustainable Energy Technologies (ICSET)*, 196–201. https://doi.org/10.1109/ICSET.2016.7811781

Chowdhury, A. H., & Mominuzzaman, S. M. (2015). Photovoltaic characteristics of single wall carbon nanotube (CNT): PCBM organic solar cell-effect of CNT chirality variation. *2015 International Conference on Electrical & Electronic Engineering (ICEEE)*, 169–172. https://doi.org/10.1109/CEEE.2015.7428247

Compton, O. C., & Nguyen, S. T. (2010). Graphene oxide, highly reduced graphene oxide, and graphene: versatile building blocks for carbon-based materials. *Small*, *6*(6), 711–723. https://doi.org/10.1002/smll.200901934

Cui, C., Li, X., Liu, J., Hou, Y., Zhao, Y., & Zhong, G. (2015). Synthesis and functions of Ag_2S nanostructures. *Nanoscale Research Letters*, *10*(1), 1–21. https://doi.org/10.1186/s11671-015-1125-7

Deibel, C., & Dyakonov, V. (2010). Polymer-fullerene bulk heterojunction solar cells. *Reports on Progress in Physics, 73*(9), 096401. https://doi.org/10.1088/0034-4885/73/9/096401

Deibel, C., Dyakonov, V., & Brabec, C. J. (2010). Organic bulk-heterojunction solar cells. *IEEE Journal of Selected Topics in Quantum Electronics*, *16*(6), 1517–1527. https://doi.org/10.1109/JSTQE.2010.2048892

Delgado, Y., Martinez, C. E., Cortez, M., Flores, N. S., & Flores, M. (2018). Optical properties of silver, silver sulfide, and silver selenide nanoparticles and antibacterial applications. *Materials Research Bulletin*, *99*, 385–392. https://doi.org/10.1016/j.materresbull.2017.11.015

Derval-Habak, H., Bergeret, C., Cousseau, J., & Nunzi, J.-M. (2009). Improving the efficiency of polymer solar cells by incorporation of functionalized SWCNTs in organic photovoltaic cells based on P3HT:PCBM photoactive layer. *2009 3rd ICTON Mediterranean Winter Conference (ICTON-MW)*, 1–4. https://doi.org/10.1109/ICTONMW.2009.5385641

Dhar, A., Naeth, M. A., Jennings, P. D., & Gamal El-Din, M. (2020). Perspectives on environmental impacts and a land reclamation strategy for solar and wind energy systems. *Science of The Total Environment*, *718*, 1–60. https://doi.org/10.1016/j.scitotenv.2019.134602

Dhuriya, D., Kumar, B., & Chauhan, R. K. (2016). Recent advancement in organic solar cells and comparison between various structures. *2016 International Conference on Emerging*

Trends in Communication Technologies (ETCT), 1–5. https://doi.org/10.1109/ETCT.2016.7882960

Farahmand, M. Z., Nazari, M. E., Shamlou, S., & Shafie-khah, M. (2021). The simultaneous impacts of seasonal weather and solar conditions on PV panels' electrical characteristics. *Energies*, *14*(4), 1–19. https://doi.org/10.3390/en14040845

Farivar, F., Lay Yap, P., Karunagaran, R. U., & Losic, D. (2021). Thermogravimetric analysis (TGA) of graphene materials: effect of particle size of graphene, graphene oxide and graphite on thermal parameters. *Journal of Carnon Research*, *7*(2), 1–12. https://doi.org/10.3390/c7020041

Guo, X., Zhou, N., Lou, S. J., Smith, J., Tice, D. B., Hennek, J. W., Ortiz, R. P., Navarrete, J. T. L., Li, S., Strzalka, J., Chen, L. X., Chang, R. P. H., Facchetti, A., & Marks, T. J. (2013). Polymer solar cells with enhanced fill factors. *Nature Photonics*, *7*(10), 825–833. https://doi.org/10.1038/nphoton.2013.207

Gupta, V., Kyaw, A. K. K., Wang, D. H., Chand, S., Bazan, G. C., & Heeger, A. J. (2013). Barium: an efficient cathode layer for bulk-heterojunction solar cells. *Scientific Reports*, *3*(1), 1965. https://doi.org/10.1038/srep01965

Gurunathan, S., Han, J. W., Park, J. H., Kim, E., Choi, Y. J., Kwon, D. N., & Kim, J. H. (2015). Reduced graphene oxide-silver nanoparticle nanocomposite: A potential anticancer monotherapy. *International Journal of Nanomedicine*, *10*, 6257–6276. https://doi.org/10.2147/IJN.S92449

Hamed, M. S. G., Adedeji, M. A., Zhang, Y., & Mola, G. T. (2020). Silver sulphide nano-particles enhanced photo-current in polymer solar cells. *Applied Physics A: Materials Science and Processing*, *126*(3), 1–207. https://doi.org/10.1007/s00339-020-3389-8

He, Z., Zhong, C., Su, S., Xu, M., Wu, H., & Cao, Y. (2012). Enhanced power-conversion efficiency in polymer solar cells using an inverted device structure. *Nature Photonics*, *6*(9), 591–595. https://doi.org/10.1038/nphoton.2012.190

Hoppe, H., Arnold, N., Sariciftci, N. S., & Meissner, D. (2003). Modeling the optical absorption within conjugated polymer/fullerene-based bulk-heterojunction organic solar cells. *Solar Energy Materials and Solar Cells*, *80*(1), 105–113. https://doi.org/10.1016/S0927-0248(03)00137-5

Hosseini, S. E., & Wahid, M. A. (2020). Hydrogen from solar energy is a clean energy carrier from a sustainable energy source. *International Journal of Energy Research*, *44*(6), 4110–4131. https://doi.org/10.1002/er.4930

Hou, X., Li, Q., Cheng, T., Yu, L., Wang, F., Lin, J., Dai, S., Li, Y., & Tan, Z. (2015). Improvement of the power conversion efficiency and long-term stability of polymer solar cells by incorporation of amphiphilic Nafion doped PEDOT-PSS as a hole extraction layer. *Journal of Materials Chemistry A*, *3*(36), 18727–18734. https://doi.org/10.1039/C5TA03967C

Hummers, W. S., & Offeman, R. (1958). Preparation of graphitic oxide. *Journal of the American Chemical Society*, *80*(6), 1339–1339.

Ibrahim, K., Saeed, K., & Khan, I. (2019). Nanoparticles: properties, applications, and toxicities. *Arabian Journal of Chemistry*, *12*(7), 908–931. https://doi.org/10.1016/j.arabjc.2017.05.011

Islam, R., Abrar, M. M., Hassan, F., & Adnan, S. (2019). Layer thickness effect on power conversion efficiency of a P3HT:PCBM based organic solar cell. *2019 1st International Conference on Advances in Science, Engineering and Robotics Technology (ICASERT)*, 1–3. https://doi.org/10.1109/ICASERT.2019.8934453

Ismail, Y. A. M., Soga, T., & Jimbo, T. (2015). Effect of composition on conjugation structure and energy gap of P3HT:PCBM organic solar cell. *International Journal of New Horizons in Physics*, *2*(2), 87–93. https://doi.org/10.12785/ijnhp/020208

Jaehoon, Kwak, E., Seo, J., Kim, H., & Kim, Y. (2016). Hybrid solar cells with polymeric bulk heterojunction layers containing inorganic nanoparticles. *IEEE Journal of Photovoltaics*, *6*(4), 924–929. https://doi.org/10.1109/JPHOTOV.2016.2553785

Jayachandran, M., Gatla, R. K., Rao, K. P., Rao, G. S., Mohammed, S., Milyani, A. H., Azhari, A. A., Kalaiarasy, C., & Geetha, S. (2022). Challenges in achieving sustainable development goal 7: Affordable and clean energy in light of nascent technologies. *Sustainable Energy Technologies and Assessments*, *53*, 1–9. https://doi.org/10.1016/j.seta.2022.102692

Jeong, Y. J., Song, J. H., Jeong, S., & Baik, S. J. (2018). PbS colloidal quantum dot solar cells with organic hole transport layers for enhanced carrier separation and ambient stability. *IEEE Journal of Photovoltaics*, *8*(2), 493–498. https://doi.org/10.1109/JPHOTOV.2017.2784766

Jinfeng, W., Chunxiu, Y., Fang, L., Xufei, M., Jiangbo, W., & Junhui, L. (2016). The development and utilization of new clean energy. *2016 IEEE International Conference on Power and Renewable Energy (ICPRE)*, 639–643. https://doi.org/10.1109/ICPRE.2016.7871156

Jiříčková, A., Jankovský, O., Sofer, Z., & Sedmidubský, D. (2022). Synthesis and applications of graphene oxide. *Materials*, *15*(3), 1–21. https://doi.org/10.3390/ma15030920

Jo, G., Na, S.-I., Oh, S.-H., Lee, S., Kim, T.-S., Wang, G., Choe, M., Park, W., Yoon, J., Kim, D.-Y., Kahng, Y. H., & Lee, T. (2010). Tuning of a graphene-electrode work function to enhance the efficiency of organic bulk heterojunction photovoltaic cells with an inverted structure. *Applied Physics Letters*, *97*(21), 213301. https://doi.org/10.1063/1.3514551

Jung, J., Kim, D., Shin, W. S., Moon, S. J., Lee, C., & Yoon, S. C. (2010). Highly efficient organic photovoltaic cells with molybdenum oxide buffer layer. *Japanese Journal of Applied Physics*, *49*(5 PART 2), 05EB05. https://doi.org/10.1143/JJAP.49.05EB05

Kalita, G., Wakita, K., & Umeno, M. (2010). Efficient bulk heterojunction solar cells incorporating carbon nanotubes and with electron-selective interlayers. *2010 35th IEEE Photovoltaic Specialists Conference*, 000090–000094. https://doi.org/10.1109/PVSC.2010.5614489

Karim, N., Mime, F. I., Islam, M. R., & Mehedi, I. M. (2017). Tandem organic solar cells with improved efficiency. *2017 International Conference on Electrical, Computer and Communication Engineering (ECCE)*, 820–825. https://doi.org/10.1109/ECACE.2017.7913016

Kesavan, A. V., Jagdish, A. K., & Ramamurthy, P. C. (2016). Light trapping and management in inverted organic solar cells employing metal nanoparticles. *2016 IEEE 43rd Photovoltaic Specialists Conference (PVSC)*, 0328–0333. https://doi.org/10.1109/PVSC.2016.7749604

Khalil, A., Ahmed, Z., Touati, F., & Masmoudi, M. (2016). Review on organic solar cells. *2016 13th International Multi-Conference on Systems, Signals & Devices (SSD)*, 342–353. https://doi.org/10.1109/SSD.2016.7473760

Khalili, D. (2016). Graphene oxide : a promising carbocatalyst for the regioselective thiocyanation of aromatic amines, phenols, anisols, and enolizable ketones by hydrogen peroxide/KSCN in water department of chemistry, college of sciences, Shiraz University, Shiraz 7. *New Journal of Chemistry*, *40*(3), 2547–2553.

Khan, F. Ullah, Mahmood, S., Ahmad, Z., Mahmood, T., & Nizami, Z. A. (2019). Graphene oxide synthesis by facile method and its characterization. *Open Journal of Chemistry*, *2*(1), 11–15. https://doi.org/10.30538/psrp-ojc2019.0008

Khanarian, G., Joo, J., Liu, X.-Q., Eastman, P., Werner, D., O'Connell, K., & Trefonas, P. (2013). The optical and electrical properties of silver nanowire mesh films. *Journal of*

Applied Physics, *114*(2), 1–15. https://doi.org/10.1063/1.4812390

Kim, Lim, K.-G., & Lee, T.-W. (2016). Planar heterojunction organometal halide perovskite solar cells: roles of interfacial layers. *Energy & Environmental Science*, *9*(1), 12–30. https://doi.org/10.1039/C5EE02194D

Koster, L. J. A., Smits, E. C. P., Mihailetchi, V. D., & Blom, P. W. M. (2005). Device model for the operation of polymer/fullerene bulk heterojunction solar cells. *Physical Review B*, *72*(8), 085205. https://doi.org/10.1103/PhysRevB.72.085205

Kumar, S., Iyer, S., & Pagare, V. (2007). Effect of annealing on poly (3-hexylthiophene) and [6,6]-phenyl C_{61}-butyric acid methyl ester bulk heterojunction solar cells. *2007 International Workshop on Physics of Semiconductor Devices*, 541–546. https://doi.org/10.1109/IWPSD.2007.4472571

Kumar, S., Kumar, J., Narayan Sharma, S., & Srivastava, S. (2019). rGO integrated MEHPPV and P3HT polymer blends for bulk heterojunction solar cells: A comparative insight. *Optik*, *178*, 411–421. https://doi.org/10.1016/j.ijleo.2018.09.148

Kumari, P., Chandran, P., & Khan, S. S. (2014). Synthesis and characterization of silver sulfide nanoparticles for photocatalytic and antimicrobial applications. *Journal of Photochemistry and Photobiology B: Biology*, *141*, 235–240. https://doi.org/10.1016/j.jphotobiol.2014.09.010

Lattante, S. (2014). Electron and hole transport layers: their use in inverted bulk heterojunction polymer solar cells. *Electronics*, *3*(1), 132–164. https://doi.org/10.3390/electronics3010132

Lenes, M., Morana, M., Brabec, C. J., & Blom, P. W. M. (2009). Recombination-limited photocurrents in low bandgap polymer/fullerene solar cells. *Advanced Functional Materials*, *19*(7), 1106–1111. https://doi.org/10.1002/adfm.200801514

Li, S.S., Tu, K.H., Lin, C. C., Chen, C.W., & Chhowalla, M. (2010a). Solution-processable graphene oxide as an efficient hole transport layer in polymer solar cells. *ACS Nano*, *4*(6), 3169–3174. https://doi.org/10.1021/nn100551j

Li, S.S., Tu, K.-H., Lin, C. C., Chen, C. W., & Chhowalla, M. (2010b). Solution-processable graphene oxide as an efficient hole transport layer in polymer solar cells. *ACS Nano*, *4*(6), 3169–3174. https://doi.org/10.1021/nn100551j

Liao, C., Erbaugh, J. T., Kelly, A. C., & Agrawal, A. (2021). Clean energy transitions and human well-being outcomes in lower and middle-income countries: A systematic review. *Renewable and Sustainable Energy Reviews*, *145*, 1–8.

https://doi.org/10.1016/j.rser.2021.111063

Liu, L., Stanchina, W. E., & Li, G. (2008). Enhanced performance of bulk heterojunction solar cells fabricated by polymer:fullerene: carbon-nanotube composites. *2008 8th IEEE Conference on Nanotechnology*, 233–236. https://doi.org/10.1109/NANO.2008.76

Liu, X. S., Bo, Z. M., Tu, W. C., Lin, M. Y., & Chen, S. L. (2017). Enhanced performance of reduced graphene oxide photodetectors by Ag nanoparticles. *2017 Eleventh International Conference on Sensing Technology (ICST)*, 1–4. https://doi.org/10.1109/ICSensT.2017.8304481

López, M. del P. L., Palomino, J. L. V., Silva, M. L. S., & Izquierdo, A. R. (2016). Optimization of the synthesis procedures of graphene and graphite oxide. In *Recent Advances in Graphene Research*. InTech. https://doi.org/10.5772/63752

Lv, D., Gordin, M. L., Yi, R., Xu, T., Song, J., Jiang, Y. B., Choi, D., & Wang, D. (2014). GeO x /reduced graphene oxide composite as an anode for Li-Ion batteries: enhanced capacity via reversible utilization of Li_2O along with improved rate performance. *Advanced Functional Materials*, *24*(8), 1059–1066. https://doi.org/10.1002/adfm.201301882

Mäckel, H., & MacKenzie, R. C. I. (2018). Determination of charge-carrier mobility in disordered thin-film solar cells as a function of current density. *Physical Review Applied*, *9*(3), 034020. https://doi.org/10.1103/PhysRevApplied.9.034020

Mahnashi, M. H., Mahmoud, A. M., Alkahtani, S. A., & El-Wekil, M. M. (2021). Ivermectin detection using Ag@B, S co-doped reduced graphene oxide nanohybrid. *Journal of Alloys and Compounds*, *871*, 1–8. https://doi.org/10.1016/j.jallcom.2021.159627

Malti, I., & Sari, N. E. C. (2014). Electrical simulation of organic solar cell based on CuPc/C60 heterojunctions. *2014 North African Workshop on Dielectric Materials for Photovoltaic Systems (NAWDMPV)*, 1–3. https://doi.org/10.1109/NAWDMPV.2014.6997618

Manzano, A., López-Naranjo, E. J., Soboyejo, W., Meas-Vong, Y., & Vilquin, B. (2015). A review on the efficiency of graphene-based BHJ organic solar cells. *Journal of Nanomaterials*, *2015*, 1–15. https://doi.org/10.1155/2015/406597

Mariotti, N., Bonomo, M., Fagiolari, L., Barbero, N., Gerbaldi, C., Bella, F., & Barolo, C. (2020). Recent advances in eco-friendly and cost-effective materials towards sustainable dye-sensitized solar cells. *Green Chemistry*, *22*(21), 7168–7218. https://doi.org/10.1039/D0GC01148G

Martínez, G. A., Sánchez-Loredo, M. G., Dorantes, H. J., Martínez, J. R., Ortega, G., & Ruiz, F. (2005). Characterization of silver sulfide nanoparticles synthesized by a simple

precipitation method. *Materials Letters*, *59*(4), 529–534. https://doi.org/10.1016/j.matlet.2004.10.043

McNeill, C. R., Westenhoff, S., Groves, C., Friend, R. H., & Greenham, N. C. (2007). Influence of nanoscale phase separation on the charge generation dynamics and photovoltaic performance of conjugated polymer blends: balancing charge generation and separation. *The Journal of Physical Chemistry C*, *111*(51), 19153–19160. https://doi.org/10.1021/jp075904m

Mime, F. I., Islam, M. R., Hossain, E., Mehedi, I. M., & Hasan, M. T. (2021). Design and performance analysis of tandem organic solar cells: effect of cell parameter. *IEEE Access*, *9*, 40665–40680. https://doi.org/10.1109/ACCESS.2021.3063810

Molla, A., Li, Y., Mandal, B., Kang, S. G., Hur, S. H., & Chung, J. S. (2019). Selective adsorption of organic dyes on graphene oxide: Theoretical and experimental analysis. *Applied Surface Science*, *464*, 170–177. https://doi.org/10.1016/j.apsusc.2018.09.056

Moraes, A. C. M. de, Araujo Lima, B., Fonseca de Faria, A., Brocchi, M., & Luiz Alves, O. (2015). Graphene oxide-silver nanocomposite as a promising biocidal agent against methicillin-resistant Staphylococcus aureus. *International Journal of Nanomedicine*, 6847–6861. https://doi.org/10.2147/IJN.S90660

Naeem, H., Tofil, H. M., Soliman, M., Hai, A., Zaidi, S. H. H., Kizilbash, N., Alruwaili, D., Ajmal, M., & Siddiq, M. (2023). Reduced graphene oxide-zinc sulfide nanocomposite decorated with silver nanoparticles for wastewater treatment by adsorption, photocatalysis, and antimicrobial action. *Molecules*, *28*(3), 1–19. https://doi.org/10.3390/molecules28030926

Najam, S., Dubey, C., & Kumar, B. (2019). Behaviour analysis of multilayer and bulk heterojunction organic solar cell with aluminium-doped zinc oxide anode layer. *2019 International Conference on Electrical, Electronics and Computer Engineering (UPCON)*, 1–5. https://doi.org/10.1109/UPCON47278.2019.8980282

Ohib, R., Arnob, S. Y., Ali, M. S., Sagor, R. H., & Amin, M. R. (2016). Metal nanoparticle enhanced light absorption in GaAs thin-film solar cell. *2016 IEEE Asia-Pacific Conference on Applied Electromagnetics, APACE 2016*, 89–93. https://doi.org/10.1109/APACE.2016.7916482

Oklobia, O. (2016). *Investigations of thermally induced morphology in P3HT/PCBM thin films: influence of composition and thermal annealing on photovoltaic properties* [Unpublished Doctoral Dissertation]. Staffordshire University.

Österbacka, R., Pivrikas, A., Juška, G., Poškus, A., Aarnio, H., Sliaužys, G., Genevičius, K., Arlauskas, K., & Sariciftci, N. S. (2010). Effect of 2-D delocalization on charge transport and recombination in bulk-heterojunction solar cells. *IEEE Journal of Selected Topics in Quantum Electronics*, *16*(6), 1738–1745. https://doi.org/10.1109/JSTQE.2010.2048746

Ou, Y., Wang, Y., Yi, L., Liang, C., & Li, Y. (2007). Organic solar cells with improved spectral coverage based on copper phthalocyanine : MEH-PPV : C_{60} bulk heterojunctions. *2007 International Nano-Optoelectronics Workshop*, 146–147. https://doi.org/10.1109/INOW.2007.4302924

Pali, B. S., & Vadhera, S. (2016). Renewable energy systems for generating electric power: A review. *2016 IEEE 1st International Conference on Power Electronics, Intelligent Control and Energy Systems (ICPEICES)*, 1–6. https://doi.org/10.1109/ICPEICES.2016.7853703

Pan, S., Liu, X., & Wang, X. (2011). Preparation of Ag_2S-Graphene nanocomposite from a single source precursor and its surface-enhanced raman scattering and photoluminescent activity. *Materials Characterization*, *62*(11), 1094–1101. https://doi.org/10.1016/j.matchar.2011.08.004

Pantho, M. J. H., Junnat, N. A., & Alam, M. J. (2014). Design and analysis the characteristics of a cost-effective polymer-based bulk heterojunction tandem solar cell. *8th International Conference on Electrical and Computer Engineering*, 516–519. https://doi.org/10.1109/ICECE.2014.7026910

Park, M., Cho, W., Lee, G., Hong, S. C., Kim, M., Yoon, J., Ahn, N., & Choi, M. (2019). Highly reproducible large-area perovskite solar cell fabrication via continuous megasonic spray coating of $CH_3NH_3PbI_3$. *Small*, *15*(1), 1–7. https://doi.org/10.1002/smll.201804005

Park, N. G., Grätzel, M., Miyasaka, T., Zhu, K., & Emery, K. (2016). Towards stable and commercially available perovskite solar cells. *Nature Energy* 1(11), 1–8. Nature Publishing Group. https://doi.org/10.1038/nenergy.2016.152

Perrozzi, F., Prezioso, S., & Ottaviano, L. (2015). Graphene oxide: from fundamentals to applications. *Journal of Physics: Condensed Matter*, *27*(1), 1–22. https://doi.org/10.1088/0953-8984/27/1/013002

Pivrikas, A., Neugebauer, H., & Sariciftci, N. S. (2010). Charge carrier lifetime and recombination in bulk heterojunction solar cells. *IEEE Journal of Selected Topics in Quantum Electronics*, *16*(6), 1746–1758. https://doi.org/10.1109/JSTQE.2010.2044978

Printz, A. D., & Lipomi, D. J. (2016). Competition between deformability and charge transport

in semiconducting polymers for flexible and stretchable electronics. *Applied Physics Reviews*, *3*(2), 1–18. https://doi.org/10.1063/1.4947428

Qazi, A., Hussain, F., Rahim, N. A., Hardaker, G., Alghazzawi, D., Shaban, K., & Haruna, K. (2019). Towards sustainable energy: a systematic review of renewable energy sources, technologies, and public opinions. *IEEE Access*, *7*, 63837–63851. https://doi.org/10.1109/ACCESS.2019.2906402

Qian, Y., & Zhang, J. (2011). Low bandgap polymers with low HOMO level for bulk heterojunction organic solar cells. *2011 International Conference on Electrical and Control Engineering*, 3516–3519. https://doi.org/10.1109/ICECENG.2011.6058453

Qiu, Y., Guo, F., Hurt, R., & Külaots, I. (2014). Explosive thermal reduction of graphene oxide-based materials: mechanism and safety implications. *Carbon*, *72*, 215–223. https://doi.org/10.1016/j.carbon.2014.02.005

Rabaia, M. K. H., Abdelkareem, M. A., Sayed, E. T., Elsaid, K., Chae, K.-J., Wilberforce, T., & Olabi, A. G. (2021). Environmental impacts of solar energy systems: A review. *Science of The Total Environment*, *754*, 1–19. https://doi.org/10.1016/j.scitotenv.2020.141989

Rafique, S., Abdullah, S. M., Shahid, M. M., Ansari, M. O., & Sulaiman, K. (2017). Significantly improved photovoltaic performance in polymer bulk heterojunction solar cells with graphene oxide/PEDOT:PSS double-decked hole transport layer. *Scientific Reports*, *7*(September 2016), 1–10. https://doi.org/10.1038/srep39555

Rahimi, H.-R., & Doostmohammadi, M. (2020). Nanoparticle synthesis, applications, and toxicity. In *Applications of Nanobiotechnology* (pp. 1–16). IntechOpen. https://doi.org/10.5772/intechopen.87973

Ram, K. S., Ompong, D., Rad, H. M., Setsoafia, D. D. Y., & Singh, J. (2021). An alternative approach to simulate the power conversion efficiency of bulk heterojunction organic solar cells. *Physica Status Solidi (A)*, *218*(2), 1–25. https://doi.org/10.1002/pssa.202000597

Ranjan, P., Agrawal, S., Sinha, A., Rao, T. R., Balakrishnan, J., & Thakur, A. D. (2018). A low-cost non-explosive synthesis of graphene oxide for scalable applications. *Scientific Reports*, *8*(1), 1–13. https://doi.org/10.1038/s41598-018-30613-4

Ratner, S. V., & Lychev, A. V. (2019). Evaluating environmental impacts of photovoltaic technologies using data envelopment analysis. *Advances in Systems Science and Applications*, *19*(1), 12–30. https://doi.org/10.25728/assa.2019.19.1.651

Ray, B., & Alam, M. A. (2012). Achieving fill factor above 80% in organic solar cells by charged interface. *2012 IEEE 38th Photovoltaic Specialists Conference (PVSC) PART 2*,

1–8. https://doi.org/10.1109/PVSC-Vol2.2012.6656773

Ray, B., & Alam, M. A. (2013). Achieving fill factor above 80% in organic solar cells by charged interface. *IEEE Journal of Photovoltaics*, *3*(1), 310–317. https://doi.org/10.1109/JPHOTOV.2012.2216508

Reichmuth, S. K., Siefer, G., Schachtner, M., Muhleis, M., Hohl-Ebinger, J., & Glunz, S. W. (2020). Measurement uncertainties in I–V calibration of multi-junction solar cells for different solar simulators and reference devices. *IEEE Journal of Photovoltaics*, *10*(4), 1076–1083. https://doi.org/10.1109/JPHOTOV.2020.2989144

Rivera-Taco, J., Castro-Beltrán, R., Maldonado, J.-L., Álvarez-Martínez, J., Barreiro-Argüelles, D., Gaspar, J. A., & Gutiérrez-Juárez, G. (2021). The role of silver nanoparticles in the hole transport layer in organic solar cells based on PBDB-T:ITIC. *Journal of Electronic Materials*, *50*(7), 4118–4127. https://doi.org/10.1007/s11664-021-08919-3

Sadovnikov, S. I., & Gusev, A. I. (2017). Recent progress in nanostructured silver sulfide: from synthesis and nonstoichiometry to properties. *Journal of Materials Chemistry A*, *5*(34), 17676–17704. https://doi.org/10.1039/C7TA04949H

Sadovnikov, S. I., & Gusev, A. I. (2018). Thermal expansion, heat capacity and phase transformations in nanocrystalline and coarse-crystalline silver sulfide at 290–970 K. *Journal of Thermal Analysis and Calorimetry*, *131*(2), 1155–1164. https://doi.org/10.1007/s10973-017-6691-8

Sakib, S. N., Rahman, S., & Parvin, S. (2017). Behavior of a physics-based p-i-n perovskite solar cell by varying different cell parameters. *2017 International Conference on Electrical, Computer and Communication Engineering (ECCE)*, 417–422. https://doi.org/10.1109/ECACE.2017.7912941

Shaban, M., Benghanem, M., Almohammedi, A., & Rabia, M. (2021). Optimization of the active layer P3HT:PCBM for organic solar cell. *Coatings*, *11*(7), 863. https://doi.org/10.3390/coatings11070863

Shamsudin, M. S., & Sanip, S. M. (2015). A Review on the two-dimensional graphene exploited in organic solar cells applications. *Advanced Materials Research*, *1109*(June), 514–518. https://doi.org/10.4028/www.scientific.net/amr.1109.514

Sharma, A., Pathak, D., Sharma, D. P., & Nunzi, J. M. (2022). Recent advances in bulk-heterojunction solar cells: a review. *The European Physical Journal Applied Physics*, *97*, 81–98. https://doi.org/10.1051/epjap/2022220113

Sharma, N., Sharma, V., Jain, Y., Kumari, M., Gupta, R., Sharma, S. K., & Sachdev, K. (2017). Synthesis and characterization of graphene oxide (GO) and Reduced graphene oxide (rGO) for gas sensing application. *Macromolecular Symposia*, *376*(1), 1–5. https://doi.org/10.1002/masy.201700006

Shiau, L. L., Goh, S. C. K., Wang, X., Zhu, M., Tan, C. S., Liu, Z., & Tay, B. K. (2019). Graphene–metal nanoparticles for enhancing thermoelectric power factor. *IEEE Transactions on Nanotechnology*, *18*, 1114–1118. https://doi.org/10.1109/TNANO.2019.2948077

Smith, C. T., Rhodes, R. W., Beliatis, M. J., Imalka Jayawardena, K. D. G., Rozanski, L. J., Mills, C. A., & P. Silva, S. R. (2014). Graphene oxide hole transport layers for large area, high efficiency organic solar cells. *Applied Physics Letters*, *105*(7), 1–6. https://doi.org/10.1063/1.4893787

Song, Z., Xu, T., Gordin, M. L., Jiang, Y., Bae, I., Xiao, Q., Zhan, H., Liu, J., & Wang, D. (2012). Polymer−graphene nanocomposites as ultrafast-charge and -discharge cathodes for rechargeable lithium batteries. *Nano Letters*, 2205–2211.

Steim, R., Kogler, F. R., & Brabec, C. J. (2010). Interface materials for organic solar cells. *Journal of Materials Chemistry*, *20*(13), 2499–2512. https://doi.org/10.1039/b921624c

Sun, F., Ghosh, H., Wang, J., Tan, Z., & Sivoththaman, S. (2022). A two-step process for reduced graphene oxide films with work function tunability. *IEEE Transactions on Nanotechnology*, *21*, 481–488. https://doi.org/10.1109/TNANO.2022.3193075

Tadeson, G., & Sabat, R. (2019). Enhancement of the power conversion efficiency of organic solar cells by surface patterning of azobenzene thin films. *2019 Photonics North (PN)*, 1–1. https://doi.org/10.1109/PN.2019.8819592

Tang, X.-Z., Li, X., Cao, Z., Yang, J., Wang, H., Pu, X., & Yu, Z.-Z. (2013). Synthesis of graphene decorated with silver nanoparticles by simultaneous reduction of graphene oxide and silver ions with glucose. *Carbon*, *59*, 93–99. https://doi.org/10.1016/j.carbon.2013.02.058

Tawalbeh, M., Al-Othman, A., Kafiah, F., Abdelsalam, E., Almomani, F., & Alkasrawi, M. (2021). Environmental impacts of solar photovoltaic systems: A critical review of recent progress and future outlook. *Science of The Total Environment*, *759*, 1–62. https://doi.org/10.1016/j.scitotenv.2020.143528

Tewatia, K., Sharma, A., Sharma, M., & Kumar, A. (2021). Synthesis of graphene oxide and its reduction by green reducing agent. *Materials Today: Proceedings*, *44*, 3933–3938.

https://doi.org/10.1016/j.matpr.2020.09.294

Tran, Q. N., Kim, J. H., & Park, S. J. (2015). Light absorption enhancement of organic solar cells with metallic plasmonic nanoparticles. *2015 20th Microoptics Conference (MOC)*, 1–2. https://doi.org/10.1109/MOC.2015.7416526

Turner, J. M. (2022). The matter of a clean energy future. *Science*, *376*(6600), 1361–1361. https://doi.org/10.1126/science.add5094

Tzolov, M., & McIntyre, M. (2017). Interface band gap and charge trapping in bulk heterojunction solar cells. *2017 IEEE 44th Photovoltaic Specialist Conference (PVSC)*, 1040–1043. https://doi.org/10.1109/PVSC.2017.8366387

Vasilevskiy, M. I., Santos, J. E., Pereira, R. M., Bludov, Y. V., Vaz, F., & Peres, N. M. R. (2016). Graphene and polarisable nanoparticles: Looking good together? *2016 18th International Conference on Transparent Optical Networks (ICTON)*, 1–4. https://doi.org/10.1109/ICTON.2016.7550390

Vi, T., Rajesh Kumar, S., Rout, B., Liu, C. H., Wong, C. B., Chang, C. W., Chen, C. H., Chen, D., & Lue, S. (2018). The preparation of graphene oxide-silver nanocomposites: the effect of silver loads on gram-positive and gram-negative antibacterial activities. *Nanomaterials*, *8*(3), 1–15. https://doi.org/10.3390/nano8030163

Virji, M. A., & Stefaniak, A. B. (2014). A review of engineered nanomaterial manufacturing processes and associated exposures. In *Comprehensive Materials Processing* (pp. 103–125). Elsevier. https://doi.org/10.1016/B978-0-08-096532-1.00811-6

Vitoratos, E., Sakkopoulos, S., Dalas, E., Paliatsas, N., Karageorgopoulos, D., Petraki, F., Kennou, S., & Choulis, S. (2009). Thermal degradation mechanisms of PEDOT:PSS. *Organic Electronics*, *10*(1), 61–66. https://doi.org/10.1016/j.orgel.2008.10.008

Wadsworth, A., Hamid, Z., Kosco, J., Gasparini, N., & McCulloch, I. (2020). The bulk heterojunction in organic photovoltaic, photodetector, and photocatalytic applications. *Advanced Materials*, *32*(38), 1–27. https://doi.org/10.1002/adma.202001763

Wang, Y., Liao, Q., Chen, J., Huang, W., Zhuang, X., Tang, Y., Li, B., Yao, X., Feng, X., Zhang, X., Su, M., He, Z., Marks, T. J., Facchetti, A., & Guo, X. (2020). Teaching an old anchoring group new tricks: enabling low-cost, eco-friendly hole-transporting materials for efficient and stable perovskite solar cells. *Journal of the American Chemical Society*, *142*(39), 16632–16643. https://doi.org/10.1021/jacs.0c06373

Wang, Z., Zhang, C., Gao, R., Chen, D., Tang, S., Zhang, J., Wang, D., Lu, X., & Hao, Y. (2014). Improvement of transparent silver thin film anodes for organic solar cells with a

decreased percolation threshold of silver. *Solar Energy Materials and Solar Cells*, *127*, 193–200. https://doi.org/10.1016/j.solmat.2014.04.024

Wen, C., Yang, Y. J., Ma, Y. J., Shi, Z. Q., Wang, Z. J., Mo, J., Li, T. C., Li, X. H., Hu, S. F., & Yang, W. B. (2019). Sulfur-hyper doped silicon nanocrystalline layer prepared on polycrystalline silicon solar cell substrate by thin film deposition and nanosecond-pulsed laser irradiation. *Applied Surface Science*, *476*, 49–60. https://doi.org/10.1016/j.apsusc.2019.01.074

Westenhoff, S., Howard, I. A., Hodgkiss, J. M., Kirov, K. R., Bronstein, H. A., Williams, C. K., Greenham, N. C., & Friend, R. H. (2008). Charge recombination in organic photovoltaic devices with high open-circuit voltages. *Journal of the American Chemical Society*, *130*(41), 13653–13658. https://doi.org/10.1021/ja803054g

Wiegers. (1971). The crystal structure of the low-temperature form of silver selenide. *American Mineralogist*, *56*, 1882–1888.

Würfel, U., Neher, D., Spies, A., & Albrecht, S. (2015). Impact of charge transport on current-voltage characteristics and power-conversion efficiency of organic solar cells. *Nature Communications*, *6*(1), 1–9. https://doi.org/10.1038/ncomms7951

Yamanari, T., Hara, K., Taima, T., Sakai, J., & Saito, K. (2006). Dye-sensitized bulk heterojunction polymer solar cells. *2006 IEEE 4th World Conference on Photovoltaic Energy Conference*, 240–243. https://doi.org/10.1109/WCPEC.2006.279434

Yilmaz, E. Ç., Yeşilyurt, M. K., Öner, İ. V., Ömeroğlu, G., & Özakin, A. N. (2017). Operational stability and degradation of organic solar cells. *Periodicals of Engineering and Natural Sciences*, *5*(2), 152–160. https://doi.org/10.21533/pen.v5i2.105

Yogeswaran, N., Shakthivel, D., Lorenzelli, L., Vinciguerra, V., & Dahiya, R. (2017). Graphene gold nanoparticle hybrid based near infrared photodetector. *2017 IEEE SENSORS*, 1–3. https://doi.org/10.1109/ICSENS.2017.8233956

Yousefi, R., & Cheraghizade, M. (2018). Semiconductor/graphene nanocomposites: synthesis, characterization, and applications. In *Applications of Nanomaterials* (pp. 23–43). Elsevier. https://doi.org/10.1016/B978-0-08-101971-9.00002-8

Yun, J.-M., Yeo, J. S., Kim, J., Jeong, H. G., Kim, D. Y., Noh, Y. J., Kim, S. S., Ku, B. C., & Na, S. I. (2011). Solution-processable reduced graphene oxide as a novel alternative to pedot:pss hole transport layers for highly efficient and stable polymer solar cells. *Advanced Materials*, *23*(42), 4923–4928. https://doi.org/10.1002/adma.201102207

Zendehdel, M., Yaghoobi Nia, N., & Yaghoubinia, M. (2020). Emerging thin film solar panels.

In *Reliability and Ecological Aspects of Photovoltaic Modules* (pp. 92–118). IntechOpen. https://doi.org/10.5772/intechopen.88733

Zhang, C., Lin, Z., Kang, E. T., & Zhu, C. (2010). Mechanism investigation and structure design of organic solar cells for improved energy conversion efficiency. *2010 10th IEEE International Conference on Solid-State and Integrated Circuit Technology*, 1276–1279. https://doi.org/10.1109/ICSICT.2010.5667634

Zhang, H., Li, Y., Zhang, X., Zhang, Y., & Zhou, H. (2020). Role of interface properties in organic solar cells: from substrate engineering to bulk-heterojunction interfacial morphology. *Materials Chemistry Frontiers*, *4*(10), 2863–2880. https://doi.org/10.1039/D0QM00398K

Zhao, Q., Xu, X., Xu, Y., Gongsun, K., Hu, L., Yan, S., Yao, W., & Yan, Z. (2020). Synergistically improved electrochemical performance and its practical application of graphene oxide stabilized nano Ag_2S by one-pot homogeneous precipitation. *Applied Surface Science*, *501*, 1–8. https://doi.org/10.1016/j.apsusc.2019.144208

Zhou, Y., Gedefaw, D. A., Hellström, S., Krätschmer, I., Zhang, F., Mammo, W., Inganäs, O., & Andersson, M. R. (2010). Black polymers in bulk-heterojunction solar cells. *IEEE Journal of Selected Topics in Quantum Electronics*, *16*(6), 1565–1572. https://doi.org/10.1109/JSTQE.2010.2049002

Zuhir, H. M., Saad, I., Roystone, A., Khairul, A. M., Ghosh, B., & Bolong, N. (2017). Enhancing efficiency of organic solar cells by interfacial materials modification. *2017 IEEE Regional Symposium on Micro and Nanoelectronics (RSM)*, 159–162. https://doi.org/10.1109/RSM.2017.8069154

APPENDICES

Appendix A: Publication Abstract

World Academy of Science, Engineering and Technology
International Journal of Materials and Metallurgical Engineering
Vol:18, No:10, 2024

Structural and Optical Properties of Silver Sulfide-Reduced Graphene Oxide Nanocomposite

Oyugi Ngure Robert, Tabitha A. Amollo, Kallen Mulilo Nalyanya

***Abstract*—**Nanomaterials have attracted significant attention in research because of their exemplary properties, making them suitable for diverse applications. This paper reports the successful synthesis as well as the structural and optical properties of silver sulfide-reduced graphene oxide (Ag_2S-rGO) nanocomposite. The nanocomposite was synthesized by the chemical reduction method. Scanning electron microscopy (SEM) showed that the reduced graphene oxide (rGO) sheets were intercalated within the Ag_2S nanoparticles during the chemical reduction process. The SEM images also showed that Ag_2S had the shape of nanowires. Further, SEM energy dispersive X-ray (SEM EDX) showed that Ag_2S-rGO is mainly composed of C, Ag, O, and S. X-ray diffraction analysis manifested a high crystallinity for the nanowire-shaped Ag_2S nanoparticles with a d-spacing ranging between 1.0 Å and 5.2 Å. Thermal gravimetric analysis (TGA) showed that rGO enhances the thermal stability of the nanocomposite. Ag_2S-rGO nanocomposite exhibited strong optical absorption in the UV region. The formed nanocomposite is dispersible in polar and non-polar solvents, qualifying it for solution-based device processing. Thus, the surface plasmon resonance effect associated with metallic nanoparticles, strong optical absorption, thermal stability crystallinity and hydrophilicity of the nanocomposite suits it for solar energy conversion applications.

***Keywords*—**Silver sulfide, reduced graphene oxide, nanocomposite, structural properties, optical properties.

biomedicine [4]. The nanoparticles of silver sulfide have also attracted optical applications within the visible region through surface plasmon resonance [4]. The Ag_2S NPs have a monoclinic crystal structure, a significant absorption coefficient [5], a narrow band gap (between 0.9 eV to 1.05 eV) [6], good chemical stability, and photoconductivity [4]. The uniqueness of these properties also makes the nanomaterials applicable in various areas, including sensors, food packaging, drug delivery, conductive paints, rechargeable batteries, and active electronic devices [7]. Nanoparticles are also applicable in energy conversion, where they offer surface plasmon resonances which enhance the trapping of light and allow for the tuning of resonant wavelengths [8]. Silver nanowire is one of the nanoparticles that are effective in trapping light through Localized Surface Plasmon Resonance (LSPR) [5]. In a nanocomposite, two nanomaterials are brought together resulting in enhanced properties since they combine the different materials' properties.

Graphene is a monolayer 2D nanomaterial of sp^2-hybridized carbon atoms densely packed in a honeycomb lattice structure [9]. Graphene has desirable mechanical properties, i.e., a break strength of 42 Nm^{-1} [10], an intrinsic tensile strength of 130.5 GPa, and 1.0 TPa Young's modulus [11] and high charge carrier

Appendix B: NACOSTI Research Permit

REPUBLIC OF KENYA

NATIONAL COMMISSION FOR SCIENCE,TECHNOLOGY & INNOVATION

Ref No: **472254**

Date of Issue: **27/January/2022**

RESEARCH LICENSE

This is to Certify that Mr.. Robert Ngure Oyugi of Egerton University, has been licensed to conduct research in Nakuru on the topic: SYNTHESIS AND CHARACTERIZATION OF SILVER SULPHIDE-GRAPHENE OXIDE NANOCOMPOSITE FOR APPLICATION IN ORGANIC SOLAR CELLS for the period ending : 27/January/2023.

License No: **NACOSTI/P/22/15198**

472254

Applicant Identification Number

Director General
NATIONAL COMMISSION FOR SCIENCE,TECHNOLOGY & INNOVATION

Verification QR Code

NOTE: This is a computer generated License. To verify the authenticity of this document, Scan the QR Code using QR scanner application.

THE SCIENCE, TECHNOLOGY AND INNOVATION ACT, 2013

The Grant of Research Licenses is Guided by the Science, Technology and Innovation (Research Licensing) Regulations, 2014

CONDITIONS

1. The License is valid for the proposed research, location and specified period
2. The License any rights thereunder are non-transferable
3. The Licensee shall inform the relevant County Director of Education, County Commissioner and County Governor before commencement of the research
4. Excavation, filming and collection of specimens are subject to further necessary clearence from relevant Government Agencies
5. The License does not give authority to tranfer research materials
6. NACOSTI may monitor and evaluate the licensed research project
7. The Licensee shall submit one hard copy and upload a soft copy of their final report (thesis) within one year of completion of the research
8. NACOSTI reserves the right to modify the conditions of the License including cancellation without prior notice

National Commission for Science, Technology and Innovation
off Waiyaki Way, Upper Kabete,
P. O. Box 30623, 00100 Nairobi, KENYA
Land line: 020 4007000, 020 2241349, 020 3310571, 020 8001077
Mobile: 0713 788 787 / 0735 404 245
E-mail: dg@nacosti.go.ke / registry@nacosti.go.ke
Website: www.nacosti.go.ke